JOURNAL OF GEOPHYSICAL RESEARCH, VOL. 102, NO. B6, PAGES 12,265–12,286, JUNE 10, 1997

Intraplate versus ridge volcanism on the Pacific-Antarctic Ridge near 37°S -111°W

Roger Hekinian,[1] Peter Stoffers, [2] Colin Devey, [2] Dietrich Ackerman,[3]
Christophe Hémond,[4] John O'Connor,[2]
Nicolas Binard, [2] and Marcia Maia [4]

Abstract. Exploration of the Foundation Volcanic Chain (33°S-131°W; 37°S-111°W) revealed the existence of different magmatic provinces with relation to their geological settings. (1) The Pacific-Antarctic Ridge (PAR) is made up of several en echelon segments where both glassy mid-ocean ridge basalts (MORBs) with low incompatible elements (K_2O<200 ppm, Zr <120 ppm and Ce <20 ppm) as well as andesites and dacites have erupted, (2) Oblique Ridges located up to 300 km from the PAR axis are topped with seamounts made up essentially of transitional (T) and enriched (E) MORBs with intermediate incompatible elements (K_2O =0.11-0.40 %, Zr =70-140 ppm and Ce =15-30 ppm), (3) the Foundation Seamounts (FS) consisting essentially of isolated volcanoes which have erupted alkalic lavas (alkali basalt, trachybasalt and trachyandesite) with high incompatible elements (K_2O (0.50-1.1 %, Zr (>150 ppm) and Ce (>48 ppm)) at about 306-1300 km from the PAR axis, (4) The Old Pacific Seamounts built on a crust older than 23 m. y. located west of longitude 124°W (> 1300 km from the PAR axis) consist of T and EMORB. On the PAR axis, extensive crystal fractionation (>65%) produced the silicic lavas. On the basis of Pacific plate reconstruction using a half spreading rate of about 50 mm/yr and integrating the observed compositional changes with respect to the structural settings, it is inferred that the last volcanic events giving rise to the FS took place at about 110 km from the PAR axis about 5 m. y. ago. The Oblique Ridges built between 5 m. y. and <1 m. y. are believed to represent ancient leaky transforms and/or large discontinuities between accreting ridge segments filled by volcanic cones during the interaction (mixing) of the enriched plume components of the FS with PAR depleted (MORB type) magmatism. The Old Pacific Seamounts built on ancient crust (>23 m. y.) with MORB volcanics comparable to those of the the Oblique Ridge-PAR provinces, could also have been formed by an interaction between the Foundation Seamount (dredge site 28) hotspot magmatism and that of an ancient accreting ridge magmatism precursor of the PAR.

Introduction

Satellite altimetric data have facilitated the detection of long volcanic chains in oceanic basins [*Sandwell,* 1984; *Sandwell and Smith,* 1995; *Haxby,* 1987; *Mayia and Diament,* 1991]. Recent work on the relationship between axial and off-axial volcanism has suggested that most volcanic structures found on ridge flanks could be related to magmatic processes taking place underneath accreting plate boundary regions [*Batiza,* 1989; *Hekinian et al.*, 1989; *Maccdonald et al.,* 1989; *Scheirer and Maccdonald,* 1993]. Recently, Shen et al. [1995] also have shown that seamounts formed up to 350 km from the South East Pacific Rise near 17°-18°S were produced from a ridge-centered mantle plume. Mantle plumes rising from a boundary layer within the mantle in the sense postulated by *White and McKenzie* [1989], *Campbell and Griffiths* [1990] and *Schilling* [1991] could give rise to ridge centered volcanic structures such as Iceland and to intraplate chains of volcanoes. The off-axial seamounts found on the flank of the mid-oceanic ridges (<100 km) could have been produced from mantle plumes related to an intraplate upwelling zone or they could represent different plumbing systems within the accreting ridge system topping distinct magma sources other than that of the mid-oceanic ridge basalts (MORBs). For example, the basalts recovered from the axial seamount caldera and adjacent off-axial plateau (4 km from the axis) near 9°31'N were attributed to separate hot magma sources [*Goldstein et al.*, 1994]. Recently, *Kerr et al.* , [1995] have challenged previous assumptions [*White,* 1985; *Zindler and Hart,* 1986; *Weaver,* 1991] that all intraplate plumes are enriched in incompatible elements. Indeed Ker et al. [1995] developed the idea that mantle plumes could have incorporated depleted residues and may also contribute to the source of MORBs.

The relationship between mantle plumes upwelling underneath spreading axis, off-axis and intraplate regions as well as ridge-centered plumes [*Schilling,* 1991)] are not well understood. The off-axis volcanoes referred to here are edifices formed on, or very near, the ridge axis (<200 km) which subsequently have moved away during spreading. In order to better constrain the temporal and spatial variations of magmatic and tectonic processes between these different

[1]Institut Français pour l'Exploitation de la Mer, Centre de Brest, Géosciences Marines, Plouzané, France.
[2]University of Kiel, Geologisch-Paläontologisches Institut, Kiel, Germany.
[3]University of Kiel, Mineralogish-petrographisches Institut, Kiel, Germany.
[4]Département Sciences de la Terre, Université de Bretagne Occidentale, Brest, France.

Paper number 96JB03856.
0148-0227/97/96JB-03856$09.00

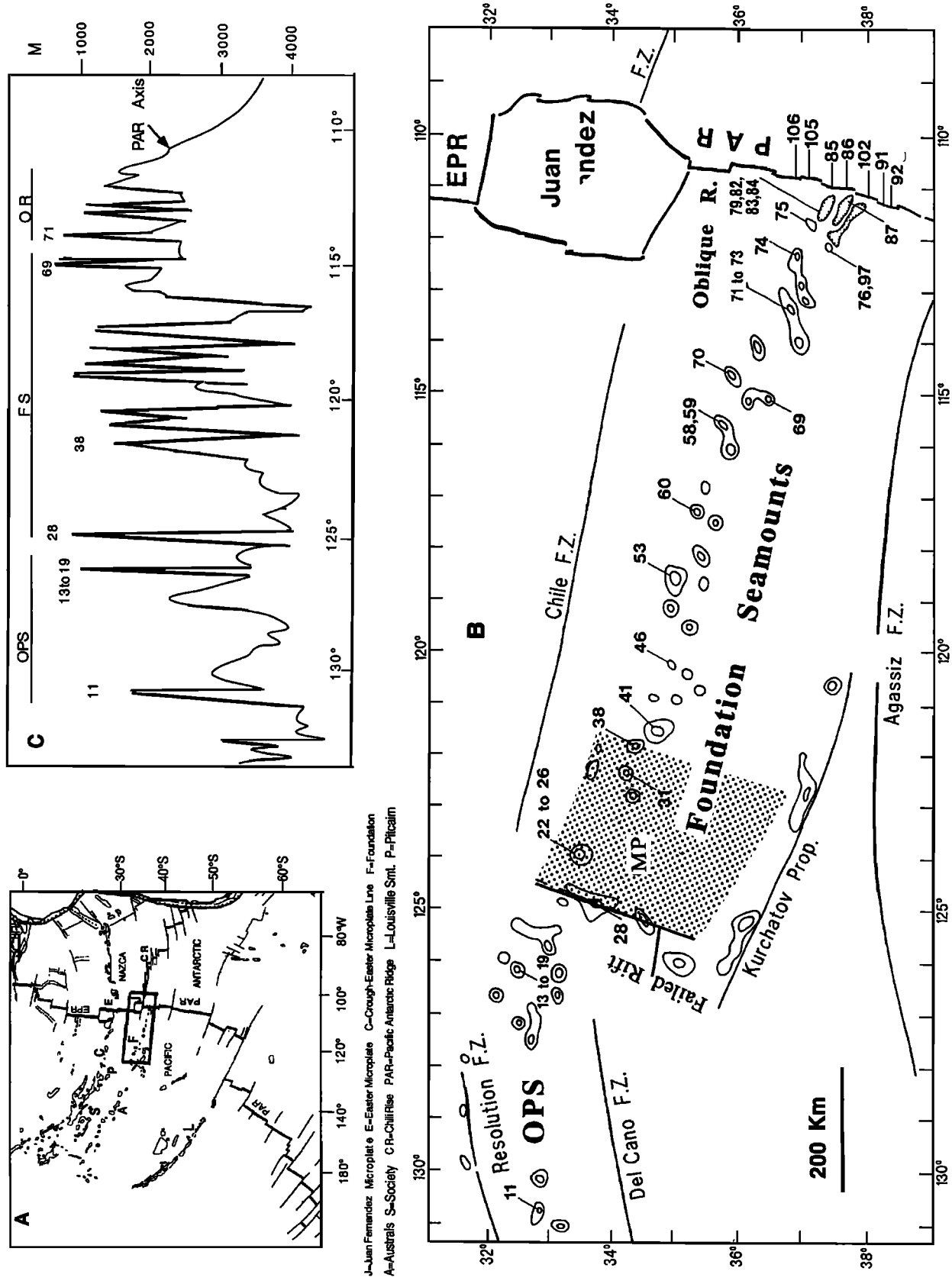
A
B
C
M
PAR Axis
OPS
F.S
O.R
11
13to19
28
38
69
71
EPR
Juan Fernandez
F.Z.
Chile F.Z.
Oblique R.
Seamounts
Foundation
MP
Failed Rift
Kurchatov Prop.
Agassiz F.Z.
Resolution F.Z.
Del Cano F.Z.
200 Km
J=Juan Fernandez Microplate E=Easter Microplate C=Crough-Easter Microplate Line F=Foundation
A=Australs S=Society CR=Chili Rise PAR=Pacific Antarctic Ridge L=Louisville Smt. P=Pitcairn

geological provinces an almost continuous volcanic chain, "the Foundation Line" [*mammerickx,* 1992] was chosen as the site of our investigations. The Foundation Line referred to here as the "Foundation Volcanic Chain" (FVC), is made up of a series of seamounts and short ridge segments located within a 180 km wide and 2000 km long band between 33°S-131°W near the Resolution fracture zone and 37°S-111°W (Pacific-Antarctic Ridge) (Figures 1a and 1b). Satellite altimetric data have provided a framework for the general tectonic and structural interpretation of this area [Craig and Sandwell, 1988; *Sandwell and Smith,* 1995; *Cande and Haxby,* 1991; Haxby and Weissel, 1986; Molnar et al., 1974; *Mammerickx,* 1992]. From a bathymetric profile, *Mammerickx* (1992) showed a topographic slope reversal (decreasing in depth towards the Resolution fracture zone) near 36°S-121°30'W, while the general seafloor topography deepens continuously from 2300 m at the Pacific-Antarctic Ridge (PAR) axis to 4300 m near 121°30'W. The area of this slope reversal was interpreted as being due to the presence of a short-lived microplate 17.5 m. y. ago [*Tebbens and Cande,* 1997] (Figures 1b and 1c).

Exploration of the volcanic chain located between the Resolution fracture zone (33°S-131°W) and the Pacific Antarctic Ridge near 37°S-111°W was undertaken during January-March 1995 with R/V *Sonne* (leg 100) as part of the French-German project of collaboration on intraplate volcanism. Extensive dredging operations on more than 25 seamounts were undertaken with bathymetric coverage limited close to the dredging stations on the seamount. A more detailed coverage made with a multichannel bathymetric survey enabled the identification of oblique linear structures as the ship approached the PAR axis. The details on the structures in relationship to the satellite altimetric data of the FVC will be presented elsewhere [*Devey et al.,* 1997]. The present work is primarily focused on the study of the compositional relationship between the PAR axial volcanism and that of the intraplate seamounts of the Foundation Volcanic Chain. We intend to show that there is a change in composition and morphology (textural) away from the PAR axis, along the FVC to the Resolution fracture zone. Inference on the location of the intraplate mantle plume and its influence on the early formation of the PAR axis is made. We also intend to show the genetic relationship between the various types of volcanics such as MORBs and to explain the rare occurrence of silicic lavas erupted along the present-day PAR axis.

Geological Provinces

Pacific-Antarctic Ridge

The geological provinces are divided into four distinct regions according to their geological settings and compositions extending from the PAR axis to the Resolution fracture zone. The first of these is the PAR axial region made up of several en echelon segments (five that we sampled), each about 30 km long separated by second- and third- order discontinuities as interpreted from multichannel bathymetric data (Figure 2). The depths along the PAR axis vary between 2230 m and 2650 m, and the summit region of the ridge crest is less than 1 km wide. Most extrusives collected from the axial zone consist of sheet flows (lobated and flat) and pillow lavas. The samples are glassy and aphyric with limited vesicularity, except for the silicic lavas which are highly vesicular and glassy with elongated cavities (dredges 91, 92, and 105). Active sulfide chimneys and temperature anomalies were detected during a deep-towed television camera survey along the PAR axis near 37°38.88'S-110°51.81'W at 2240 m depths [*Devey et al.,* 1997]. The summit of the ridge in this area is gashed by a central graben 300 m wide and 50 m deep. A dredge (86) taken about 15 km farther north of the deep-towed area contained sulfides made up of pyrite, sphalerite, calcite, and barite (Figure 2).

Rock types. The PAR samples are characterized by silicic lavas and various types of MORB (Table 1). Silicic lavas are rare on accreting ridge systems. In the eastern Pacific, only a few cases have been documented, such as on a 25-30 m. y. old crust on the flank of the North East Pacific Rise (NEPR) at 9°30'N and 10°30'N [*Langmuir et al .,* 1986; *Thompson et al.,* 1989; *Batiza et al.,* 1996]. Other andesites have been recovered from the 95°W propagator of the Galapagos Spreading Center [*Clague et al.,* 1981], along the South East Pacific Rise (SEPR) near 14°S [*Sinton et al.,* 1991] and on the Mid-Atlantic Ridge [*Aumento,* 1969].

Dacite: The dacites found in dredge hauls 91 and 86 are dark gray, glassy aphyric lava flows with a bread crumb surface texture. They form thick (about 22 cm) massive flows with a lobated appearance. Large, empty cavities (up to 1 cm in length) and small vesicles (10-18%) oriented in the main flow directions are abundant. The lava consists of plagioclase (andesine An_{35-50}), Mg-poor olivine, and titanomagnetite (samples 91-01, 91-05, 91-06) (Table 1).

Andesite: The andesites found in two dredge hauls (105 and 92) consist of a lobated flow with relatively thick (10-15 mm), glassy crust . The glassy surface was layered in different colors, going from deep blue to light brown and greenish gray,when first brought on deck of the ship. After few a weeks the various colors faded away and gave rise to a homogeneous dark grey normal glassy appearance. The glassy rocks consist of spherules with centers of crystallization (mainly plagioclase needles) and interstitial small vesicles throughout the spherules. Some plagioclase phenocrysts were analyzed and consist of oligoclase-andesine (An_{20-50}). Fe-rich olivine (Fo_{30-40}) crystals were also encountered. The analyzed glass shows a high SiO_2 (55-58%) and a high total alkali content

Figure 1. (a) Regional map of the South Pacific. (b) Map showing the distribution of volcanic structures and sample stations located between the Resolution fracture zone and the Pacific-Antarctic Ridge (PAR) which correspond to the Foundation Volcanic Chain, also called the "Foundation Line" by *Mammerickx,* [1992]. The contour lines of the major positive structures were retraced from satellite altimetric data after *Sandwell* [1984], *Haxby* [1987], and *Mayia and Diament* [1991]. The solid line near 35°S-125°W represent the trace of the failed rift [*Mammerickx,* 1992]. The inferred orientation of this failed west rift (West Rift) was chosen to follow that of the seamount line defined from satellite altimetry. The east rift corresponds to the location of the slope reversal near 35°S-121°40'W (near dredge 38) defined by *Mammerickx* [1992] and might represent the area of an ancient microplate (shaded area) [*Tebbens and Cande,* 1997]. The numbers indicate dredge stations (e.g., 11). (c) Sketched bathymetric depth profile reconstructed after the vertical beam of the multichannel echo sounder (Hydrosweep) of the R/V *Sonne* (leg 100). The vertical exaggeration is about 150.

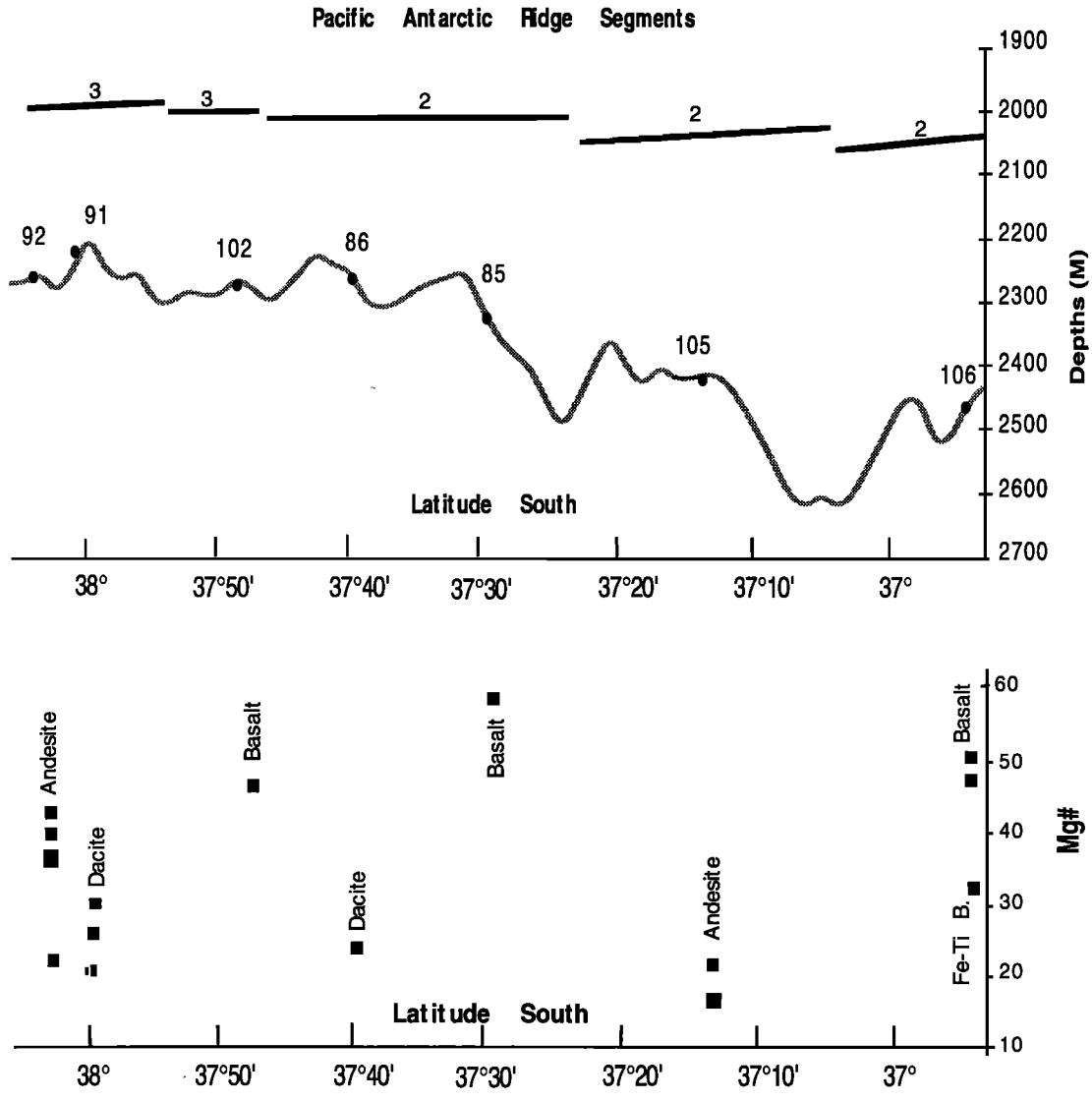

Figure 2. Bathymetric profile constructed from the multichannel (*Hydrosweep) echo sounder data obtained during the R/V* Sonne cruise (leg 100) in 1995 in the South Pacific. (a) The dredge stations indicated along the profile, with subhorizontal bars showing the structural discontinuities of second-order (overlapping spreading center) and third-order (small fissural offsets) discontinuities. (b) Rock compositional variations based on the magnesium number (Mg #) ($Mg^{2+}/Mg^{+2}+Fe^{2+}$) ratios.

(Na_2O+ K_2O) (3-4%) (Table 2). The silicic lavas are also characterized by higher light rare earth elements (REE) contents (La=25-40 ppm, Ce=60-91 ppm, and Nd=44-55 ppm).

The diversity in composition between the andesites from dredge hauls 105 and 92 (samples 92-03, 92-02, 92-04) (Table 2 and Figures 3a and 3c) is shown by the higher K_2O (0.70%) and Na_2O (3.0-3.6%), higher magnesium number (Mg #) (38-42), lower TiO_2 (1.4%), and lower FeO (9-10 %) for the samples from dredge haul 92, except for sample 92-01, which is comparable to those from station 105. This diversity also corresponds to the higher anorthite (An_{50-71}) content of the plagioclase (labradorite) for the andesites from dredge 92 with respect to the samples (An_{20-50}, oligoclase-andesine) from dredge 105.

Basalts: The glassy basalts are essentially normal (N) (sample 106-01), and transitional (T) MORBs according to the classification adopted by *Hekinian et al.*, [1989]. The glassy margins of the N MORBs (sample 106-01) consist of low K_20 (0.11%), K/Ti (<0.12), and Na_2O + K_2O (2.61%), and the T MORBs (samples 102-1 and 85-01) have a K_20 of 0.17%, Na_2O + K_2O near 3%, and K/Ti ratios of 0.11-0.25 (Table 2 and Figure 5a-5d). One Fe-Ti enriched basalt (sample 106-02) consists of high TiO_2 (3.4%) and FeO^T (16.3%) contents (Table 2). This sample (106-02) contains early formed clinopyroxene, plagioclase (An 45-60, andesine-labradorite) and olivine. The bulk trace element analyses show Zr (100-120 ppm), Y (29-40 ppm) and light REE (La=4-6 ppm, Ce=12-16 ppm and Nd=10-13 ppm) comparable to other SEPR N- and T- MORBs (Table 3; Figures 7a-7d).

Magmatic processes. Crystal fractionation in the various types of rocks encountered is evidenced from the changes in the olivine and plagioclase composition of early formed crystals in the the glass [*Schuster,* 1996]. A positive correlation between the forsterite (Fo_{30-75}) and anorthite (An_{20}-An_{75}) contents of olivine and plagioclase with the Mg

Table 1. Locations of Samples Collected by the R/V Sonne During the 1995 Cruise (Leg 100) From the Pacific-Antarctic Ridge and From Intraplate Provinces in the South Pacific Near 37°S

Sample	Province	Latitude S, Longitude W	Depth, m	Description
11-06	Old Pacific	32°56'.414, 130°45'.459	2884-3347	aphyric basalt, pl, olv
18-01	Old Pacific	32°28'.871, 126°00'.456	3010-3416	aphyric basalt, pl, olv
25-01	Foundation	33°20'.764, 123°52'.525	1669-1508	aphyric vesic.trachy andesite
28-01	Foundation	33°41'.735, 124°54'.612	467-501	phyric picritic basalt, olv ~5-9%
38-01	Foundation	34°19'.119, 121°58'.729	3469-3668	aphyric vesic.trachy basalt
38-02	Foundation	34°19'.119, 121°58'.729	3469-3668	phyric,vesic. basalt, <15% pheno. pl.
41-04	Foundation	34°52'.352, 121°33'.309	1726-2050	phyric,vesic. basalt, >15% pheno. olv, pl
46-01	Foundation	34°57'.336, 120°24'.490	3142-3731	phyric vesic. basalt >20% pheno. olv, pl.
46-02	Foundation	34°57'.336, 120°24'.490	3142-3731	phyric vesic. basalt >20% pheno olv, pl .
58-04	Foundation	35°30'.433, 116°49'.269	1580-1627	phyric vesic. basalt>10% pheno. pl.
60-05	Foundation	35°27'.003, 117°11'.833	2083-2417	phyric vesic. basalt >20% pheno. olv, pl.
69-01	Foundation	36°33'.804, 115°16'.627	2964-3288	aphyric basalt, olv, pl.
70-01	Foundation	36°20'.907, 113°55'.696	2217-2278	phyric vesic. basalt, <10% pheno.
71-01	Oblique Ridge	36°40'.812, 113°28'.350	2558-2944	moderetely phyric basalt
74-02	Oblique Ridge	36°56'.987, 112°12'.875	1637-2197	picritic basalt, olv.~7-10 %
74-03	Oblique Ridge	36°56'.987, 112°12'.875	1637-2197	picritic basalt, olv.~10 %
74-04	Oblique Ridge	36°56'.987, 112°12'.875	1637-2197	hyaloclastite (glass fragments)
75-01	Oblique Ridge	37°16'.680, 111°51'.521	2114-2647	aphyric basalt
76-04	Oblique Ridge	37°22'.140, 112°06'.098	1532-1710	aphyric basalt
78-01	Oblique Ridge	37°21'.810, 111°45'.460	2103-2489	aphyric basalt
79-06	Oblique Ridge	37°25'.109, 111°26'.093	2465-2664	aphyric basalt
82-02	Oblique Ridge	37°27'.530, 111°12'.654	1559-2128	aphyric basalt, plag., olv.
83-01	Oblique Ridge	37°24'.621, 111°24'.309	1567-1703	moderately phyric basalt
84-01	Oblique Ridge	37°27'.477, 111°03.582	2100-2315	phyric vesicular basalt
87-01	Oblique Ridge	37°38'.141, 111°17'.397	1658-1818	aphyric basalt
85-01	PAR axis	37°29'.209, 110°48'.196	2259-2261	aphyric basalt
86-02	PAR axis	37°39'.585, 110°52'.457	2222-2238	aphyric glassy basalt
91-01	PAR axis	38°05'.499, 111°00'.161	2193-2200	aphyric dacite, pl, olv, cpx,Ti-Mt
91-05	PAR axis	38°05'.499, 111°00'.161	2193-2200	aphyric vesic. dacite, pl, Ti-Mt
91-06	PAR axis	38°05'.499, 111°00'.163	2193-2200	aphyric dacite, pl, olv, cpx,Ti-Mt
92-01	PAR axis	38°09'.350, 111°02'.610	2253-2264	aphyric glassy andesite
92-02	PAR axis	38°09'.350, 111°02'.610	2253-2264	aphyric glassy andesite
92-03	PAR axis	38°09'.350, 111°02'.610	2253-2264	aphyric glassy andesite
92-04	PAR axis	38°09'.350, 111°02'.610	2253-2264	aphyric glassy andesite
102-01	PAR axis	37°46'.200, 110°54'.530	2250-2277	aphyric vesicular basalt
105-02	PAR axis	37°11'.464, 110°42'.410	2398-2419	aphyric glassy andesite
105 03	PAR axis	37°11'.464, 110°42'.410	2398-2419	aphyric glassy andesite
106-01	PAR axis	36°54'.399, 110°37'.911	2455-2494	aphyric basalt, olv, pl
106-02	PAR axis	36°54'.399, 110°37'.911	2455-2494	ferrobasalt (Fe-Ti), cpx, olv, pl

The phyric rocks contain more than >10-20% phenocrysts (mainly pl.); moderately phyric is < 8% phenocrysts. The aphyric rocks contain <1% of early formed crystals. Foundation and Old Pacific refer to seamounts . PAR is Pacific-Antarctic Ridge. Abbreviations are olv, olivine; pl, plagioclase; cpx, clinopyroxene, Ti-Mt, titanomagnetite, and vesic, vescles.

(20-63) of their associated glass was observed. Some plagioclase in the andesite (sample 92-03) showing low anorthite values for a relatively high Mg # (41-52) may be the result of mixing between evolved (i.e. sample 105-02) and less evolved MORBs. The andesites (samples 105-01, 106-02 and 105-03) and the dacites (samples 86-02, 91-05, 91-06, 91-01) show the lowest anorthite (An_{20-50}) and forsterite (Fo_{30-40}) content among the lava erupted. The Fe-Ti enriched basalts have an intermediate anorthite (An_{45-60}) and forsterite (Fo_{60}) content between the dacite-andesites and the MORBs [*Schuster*, 1996]. The basalt-andesite suites from other NEPR and SEPR regions [*Batiza et al.*, 1996] show a similar pattern of crystal fractionation to that of the PAR volcanics.

The algorithms of *Weaver and Langmuir* [1990], *Nielsen* [1988, 1990] and *Nielsen and Delong* [1992] are used to model the crystal fractionation paths of the glassy rocks comprising the MORBs, Fe-Ti basalts (sample 106-2) and silicic lavas. The calculated crystal fractionation trends observed for the FeO^T, TiO_2, SiO_2, and CaO/Al_2O_3 values with respect to the Mg # reveal that after about 65% crystallization there is a sudden change in the path of crystallization with an increase in the SiO_2 (55-65 %) and alkali content in the liquid (Figures 3a-3c). This gives rise to a decrease in TiO_2 from 3.5% to 2 % and lower. The maximum enrichment in FeO and TiO_2 (16% and 3.5% respectively) occurs at MgO = 4 % (Mg # 30-33) (Figure 3c and 3d). Other andesites (sample 92-03) and dacites (sample 86-02 and 91-01) depart from the main trend of fractionation (Figures 3a-3c).

A change in the trend of crystal fractionation for silicic lavas is strongly dependent on the oxygen fugacity (fO_2) of the melt as was shown from previous experimental work [*Sack et al.*, 1980; *Juster et al*, 1989; *Christie et al.*, 1986] as well as from the compositional variation of natural basaltic glass [*Carmichael and Ghiorso*, 1986; *Byers et al.*, 1984]. The trend of variability from basic to silicic lava is affected by the iron redox state of the liquid and depends on the oxygen fugacity (fO_2) of the magma. A survey of Pacific basalts [*Carmichael and Ghiorso*, 1986; *Christie et al.*, 1986] showed that most glassy margin MORBs have a low $Fe^{3+}/\Sigma Fe$ ratio of 0.07±3

Table 2. Average Glass Analyses From Various Rock Types Collected From the Pacific-Antarctic Ridge

	Andesite								dacite				T MORB	N MORB	FeTi B	T MORB	E MORB	
	105-01	105-01b	105-02	105-03	92-01	92-02	92-03	92-04	86-02	91-05	91-06	91-01	102-01	106-01	106-02	85-01	Cy82 09-03	
																	average	standard deviation
Average	3	8	3	6	3	6	4	4	4	4	3	4	3	6	4	3	25	
SiO_2	55.49	55.75	56.45	55.72	56.93	57.69	56.69	56.57	61.14	64.03	63.78	61.38	50.38	50.90	51.06	51.06	50.32	0.33
TiO_2	2.03	2.09	1.98	2.01	1.94	1.47	1.42	1.47	1.20	1.13	1.12	1.25	1.73	1.62	3.47	1.54	1.80	0.06
Al_2O_3	11.88	12.06	12.15	12.45	12.82	13.70	14.17	14.11	13.55	13.26	13.22	13.46	14.17	14.09	12.17	14.28	16.19	0.31
FeO*	15.66	15.81	15.51	14.86	14.03	9.82	10.14	9.79	9.51	8.60	8.82	9.01	11.45	11.23	16.33	9.96	8.61	0.22
MnO	0.30	0 34	0 31	0.25	0.26	0 20	0.17	0 18	0.22	0.18	0.16	0.19	0 18	0.21	0.32	0.18	0.15	0.06
MgO	2.01	2.01	1.96	1.61	1.90	3.08	3.63	3.55	1.78	1.34	1.40	1.98	6.75	7.14	4.07	7.22	7.51	0.21
CaO	6.37	6.28	6.29	6.16	6.18	6.54	7.23	7.21	5.01	4.33	4.51	5.56	11.01	11.23	8.64	11.62	11.02	0.14
Na_2O	2.54	2.50	2.29	2.01	2.39	3.08	3.56	3.41	2.97	3.28	3.07	2.47	2.81	2.51	2.19	2.76	3.19	0.09
K_2O	0.60	0.58	0.60	0.60	0.62	0.80	0.72	0.68	1.02	1.17	1.11	1.04	0.17	0.11	0.44	0.17	0.43	0.03
P_2O_5	0.76	0.69	0.84	0.72	0.69	0.33	0.37	0.38	0.34	0.33	0.30	0.39	0.16	0.14	0.45	0.14	0.24	0.06
Total	97.70	98.14	98.41	96.67	97.05	96.75	98.14	97.49	96.76	97.72	97.52	96.75	98.86	99.25	99.20	99.02	99.61	
Mg #	20.3	20.2	20.0	17.7	21.1	38.3	41.5	41.8	27.0	23.5	24.0	30.4	53.9	55.7	33.0	58.9	63.3	0.7
K/Ti	0.41	0.38	0.42	0.41	0.45	0.75	0.70	0.64	1.17	1.43	1.38	1.15	0.14	0.09	0.17	0.16	0.33	0.03
Na_2O+K_2O	3.14	3.08	2.89	2.60	3.02	3.88	4.27	4.09	3.99	4.45	4.18	3.51	2.99	2.61	2.63	2.94	3.61	0.09

T is transitional, N is normal, MORB, mid ocean ridge basalt, E is enriched, FeTi is Fe-Ti enriched basalt. Heading numbers refer to sample numbers. Average refer to average number of samples. The analyses were done with the SX 50 Camebax (Institut Français pour la Recherche et l'Exploitation de la Mer, Brest France). The analytical precisions are also given by Hekinian et al. [1995b]. Standard deviations were calculated from sample Cy82-09-03 used as internal standard [Hekinian et al., 1995b]. Mg #=$Mg^{2+}/Mg^{2}+Fe^{2+}$ with $Fe^{2+}/Fe^{2+}+Fe^{3+}=0.9$. The silicic lavas contain volatiles.

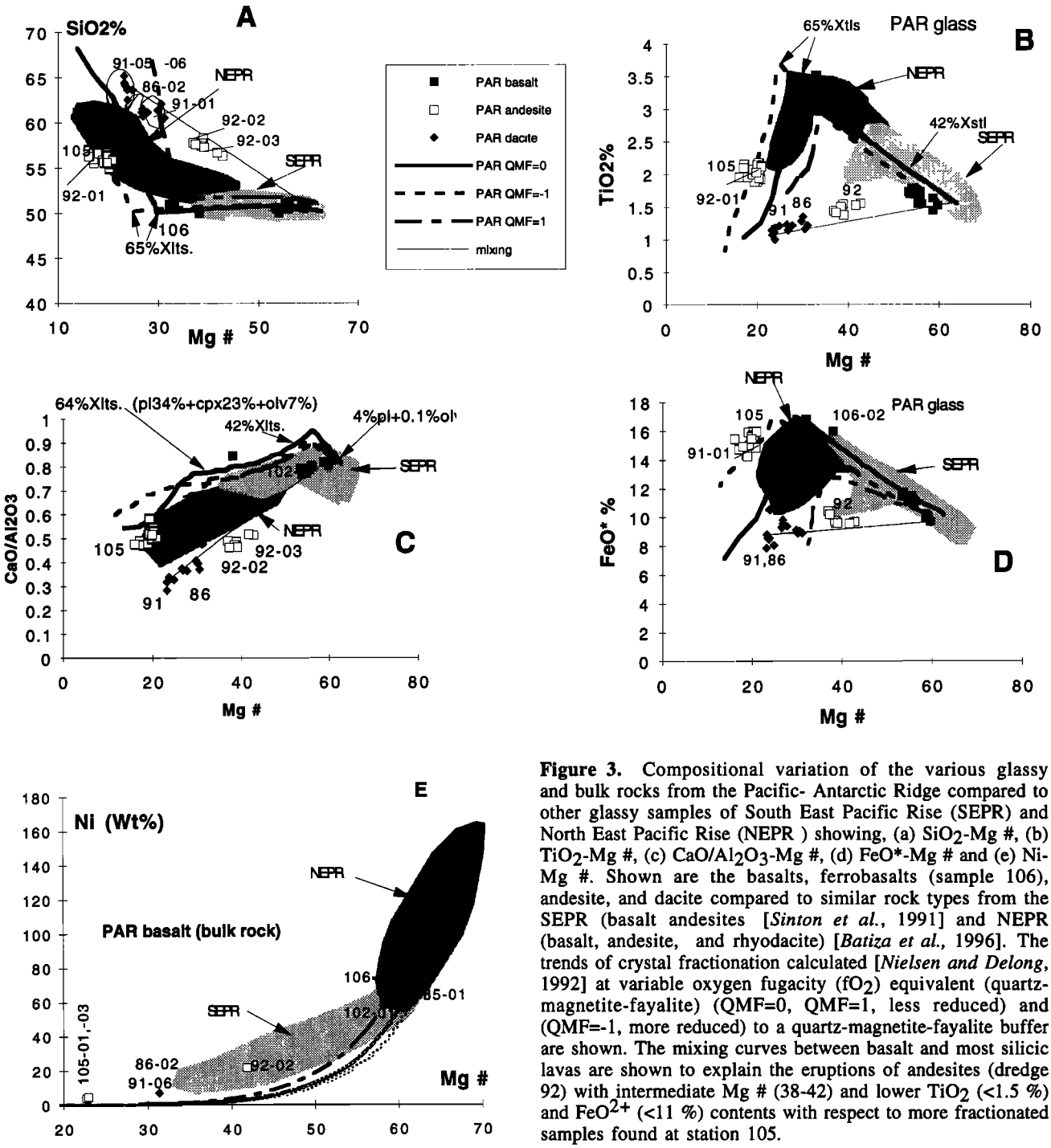

Figure 3. Compositional variation of the various glassy and bulk rocks from the Pacific- Antarctic Ridge compared to other glassy samples of South East Pacific Rise (SEPR) and North East Pacific Rise (NEPR) showing, (a) SiO_2-Mg #, (b) TiO_2-Mg #, (c) CaO/Al_2O_3-Mg #, (d) FeO*-Mg # and (e) Ni-Mg #. Shown are the basalts, ferrobasalts (sample 106), andesite, and dacite compared to similar rock types from the SEPR (basalt andesites [*Sinton et al.*, 1991] and NEPR (basalt, andesite, and rhyodacite) [*Batiza et al.*, 1996]. The trends of crystal fractionation calculated [*Nielsen and Delong*, 1992] at variable oxygen fugacity (fO_2) equivalent (quartz-magnetite-fayalite) (QMF=0, QMF=1, less reduced) and (QMF=-1, more reduced) to a quartz-magnetite-fayalite buffer are shown. The mixing curves between basalt and most silicic lavas are shown to explain the eruptions of andesites (dredge 92) with intermediate Mg # (38-42) and lower TiO_2 (<1.5 %) and FeO^{2+} (<11 %) contents with respect to more fractionated samples found at station 105.

equivalent to 1-2 $\log_{10}$ unit below the quartz-magnetite-fayalite (QMF) buffer. This buffer was used in experiments to control the oxidation of iron during crystallization [*Wones and Gilbers*, 1969]. The lavas from the PAR axis show a $Fe^{3+}/\Sigma Fe$ varying between 0.06 and 0.16 which is equal to fO_2 values of 1 to -3 $\log_{10}$ units below that of the QMF buffer (Figures 5a and 5b).

The oxygen fugacity (fO_2) is controlled by the oxidation of FeO to Fe_2O_3 and the crystallization of titanomagnetite (Ti-Mt). The passage from the Fe-Ti basalts to the andesite (samples 105-02 and 105-01) and dacite lavas is mainly emphasized by the crystallization of Ti-Mt. In a closed system this will lower the fO_2 of the melt with respect to the QMF buffer (-1, more reduced) and give rise to the andesite of sample 92-01 and of dredge 105 (Figures 5a and 5b). The $Fe^{3+}/\Sigma Fe$ of these andesites (samples 105-01 and 105-02) is lower (0.06-0.11) than the other silicic lavas (Table 4 and Figure 5a). Instead, the dacites (samples 91-01, 91-06 and 86-02) and the andesite 92-02 plotting near to and on the QMF buffer curve (=0, more oxidized) contain Ti-magnetite and also have higher $Fe^{3+}/\Sigma Fe$ (0.13-0.16) ratios of their melt than the other andesites from dredge 105 and sample 92-01 (0.06-0.11) (Figure 5a). The Fe^{3+}/Σ Fe ratios of the bulk rock basalts from the PAR area (0.09-0.12) are as low as those

Table 3. Average Glassy Basalts From Off-Axis and Intraplate Volcanoes in the South Pacific Between 33°S-131°W and 37°S-111°W

	Old Pacific Seamounts		Foundation Seamounts							Oblique Ridges										
	T MORB	E MORB	Alkali Basalt							E MORB			N MORB			T MORB				
	11-06	18-01	38-02	46-01	46-02	58-04	60-05	69-01	70-01	71-01	71-02	76-04	74-01	74-02	74-03	75-01	78-01	82-02	83-01	84-01	87-01
Average	11	8	3	8	6	10	3	8	4	6	4	3	5	8	6	3	5	2	3	4	4
SiO_2	49.68	49.18	47.32	48.34	48.84	48.30	48.79	48.45	49.45	49.85	49.65	49.03	45.97	46.75	46.26	49.41	49.13	48.90	49.65	50.39	50.49
TiO_2	1.90	2.49	4.55	3.30	2.72	2.31	3.31	2.93	2.66	2.12	2.23	1.98	0.77	0.78	0.79	1.33	1.32	1.53	1.36	1.79	2.29
Al_2O_3	14.23	13.56	13.76	14.67	14.51	14.71	13.83	14.58	14.20	14.04	14.00	14.52	17.29	17.21	17.09	14.99	15.19	15.18	14.82	14.05	13.64
FeO*	10.68	12.59	13.29	11.20	11.08	10.61	12.74	10.64	11.90	12.24	12.48	10.69	11.35	11.49	11.44	9.31	9.68	9.74	9.92	10.87	11.74
MnO	0.21	0.24	0.20	0.14	0.20	0.18	0.22	0.24	0.26	0.20	0.22	0.18	0.20	0.19	0.18	0.16	0.13	0.16	0.16	0.22	0.13
MgO	6.94	5.72	4.61	5.15	6.05	6.42	4.85	5.55	6.13	5.88	5.83	6.77	9.07	9.16	9.09	7.71	7.99	7.75	7.72	6.86	6.20
CaO	11.56	10.32	9.30	9.50	10.36	10.75	9.65	10.34	10.69	10.35	10.33	11.81	11.07	10.97	11.02	12.77	12.63	12.35	12.02	11.43	10.57
Na_2O	3.04	3.55	3.16	3.60	3.38	3.25	3.35	3.53	3.05	3.20	3.28	2.96	2.67	2.51	2.56	2.48	2.40	2.91	2.57	2.96	3.24
K_2O	0.18	0.39	1.03	0.99	0.65	0.53	0.88	0.75	0.55	0.33	0.36	0.36	0.05	0.02	0.03	0.11	0.16	0.13	0.18	0.18	0.38
P_2O_5	0.18	0.31	0.66	0.61	0.45	0.29	0.50	0.44	0.38	0.27	0.21	0.24	0.04	0.05	0.04	0.15	0.13	0.13	0.15	0.16	0.25
Total	98.64	98.36	97.87	97.51	98.24	97.34	98.14	97.47	99.27	98.48	98.60	98.56	98.52	99.11	98.58	98.42	98.79	98.80	98.60	98.91	98.92
Mg #	56.3	47.4	40.7	47.7	52.0	54.5	43.0	50.8	50.5	48.8	48.1	55.6	61.3	61.2	61.2	62.1	62.0	61.2	60.7	55.6	51.1
K/Ti	0.13	0.22	0.31	0.42	0.33	0.32	0.37	0.35	0.29	0.21	0.23	0.25	0.09	0.03	0.05	0.12	0.17	0.12	0.18	0.14	0.23
Na_2O+K_2O	3.19	3.92	4.19	4.46	4.03	3.78	4.23	4.33	3.60	3.53	3.64	3.32	2.72	2.52	2.59	2.59	2.56	3.04	2.75	3.14	3.62
Distances km	1853	1438	1052	901	901	568	619	411	306	248	248	109	137	137	137	100	82	27	36	20	35

See Table 2 descriptions. The distances from the Pacific-Antarctic Ridge axis are reported in kilometers. Samples from dredge station 74 contain abundant olivine (>5%) and spinels.

Table 4. Bulk Rock Analyses From the Pacific-Antarctic Ridge Near 37°30'S

	T MORB				Andesite			Dacite	
	85-01*	85-01	102-01	106-01	92-02	105-01	105-03	86-02	91-06
SiO_2	50.60	49.74	49.56	49.91	55.94	53.48	53.79	59.21	60.19
TiO_2	1.53	1.56	1.80	1.55	1.41	2.05	2.04	1.24	1.13
Al_2O_3	14.60	14.89	14.86	14.81	13.82	12.08	12.22	13.65	13.34
Fe_2O_3	nd	1.12	1.37	1.53	1.66	1.08	1.78	1.35	1.60
FeO	10.12	9.04	9.93	9.80	8.49	13.83	13.10	8.14	7.28
MnO	0.19	0.17	0.19	0.19	0.16	0.29	0.28	0.15	0.14
MgO	7.30	7.48	7.02	7.38	3.08	2.05	1.97	1.88	1.59
CaO	11.90	12.01	11.32	11.17	6.31	6.14	6.09	4.86	4.48
Na_2O	2.74	2.82	2.92	2.57	4.90	3.93	4.08	5.18	5.24
K_2O	0.17	0.17	0.18	0.09	0.82	1.01	0.94	1.09	1.10
P_2O_5	0.17	0.27	0.28	0.25	0.40	0.68	0.70	0.38	0.36
CO_2	nd	0.26	0.20	0.12	0.46	0.23	0.28	0.28	0.84
$H2O^+$	nd	0.31	0.38	0.40	1.51	2.14	1.54	1.73	1.72
$H2O^-$	nd	0.05	0.09	0.08	0.10	0.56	0.67	0.12	0.27
Total	99.80	99.72	99.91	99.67	98.90	99.26	99.20	99.11	99.14
Rb, ppm	1.9	2.5	3.1	1.6	12.4	12.4	12.8	17.9	16.7
Sr	153.0	143.0	137.0	86.4	109.0	133.0	133.0	105.0	97.7
Ba	28.0	28.8	31.0	15.0	94.7	104.0	105.0	146.0	129.0
V	303.0	308.0	320.0	317.0	128.0	30.3	30.0	81.3	50.5
Cr	249.0	190.0	144.0	210.0	54.2	146.0	116.0	9.8	3.5
Co	41.0	40.0	39.9	39.8	22.0	20.4	20.0	17.5	13.8
Ni	64.0	67.0	62.1	82.1	21.9	4.1	4.8	10.3	7.2
Y	29.0	28.8	33.0	39.4	100.0	99.8	100.0	103.0	113.0
Zr	91.0	100.0	121.0	110.0	580.0	388.0	393.0	642.0	704.0
Nb	6.7	6.4	7.5	4.3	24.7	25.3	26.1	33.9	33.2
La	6.1	5.9	6.7	4.6	30.9	24.5	24.9	39.5	40.3
Ce	15.0	15.4	17.6	12.8	75.0	61.5	64.0	94.7	94.9
Nd	12.0	11.4	12.9	10.9	47.9	45.3	44.0	55.1	58.9
Eu	1.2	1.3	1.4	1.4	2.7	4.1	4.0	2.9	3.2
Dy	4.9	4.4	5.1	5.7	15.1	16.6	16.6	15.8	16.8
Er	3.0	2.6	3.1	3.6	9.0	9.3	9.5	9.8	10.6
Yb	2.9	2.5	3.3	4.1	10.7	10.3	10.0	10.9	12.4
Th	0.6	0.4	0.5	0.4	3.6	1.8	1.8	4.8	4.9
Mg #	60.70	62.10	58.34	59.86	41.81	22.70	22.95	31.39	30.20
Zr/Y	3.14	3.47	3.67	2.79	5.80	3.89	3.93	6.23	6.23
K/Ti	0.15	0.15	0.14	0.08	0.81	0.68	0.64	1.22	1.35
Ce_N	24.5	25.2	28.7	21.0	122.5	100.5	104.6	154.7	155.1
Yb_N	17.0	14.9	19.2	24.2	63.1	60.6	58.9	64.2	72.8
$(Ce/Yb)_N$	1.44	1.69	1.49	0.87	1.94	1.66	1.78	2.41	2.13
$Fe^{3+}/\sum Fe$	n.d	0.10	0.11	0.12	0.15	0.07	0.11	0.13	0.17

See Table 2 descriptions. Here nd refers to no data.

The analyses were performed at the Centre Pétrographique et Géochimique, (CRPG), Nancy, France, by induced couple plasma mass spectrometry). The accuracy of the methods is given by *Govindaraju* [1989].

* Sample 85-01* was analyzed by inductively coupled plasma emission spectrometer by J. Cotten at Université de Bretagne Occidentale, Geology Department (Brest). FeO is calculated as total Fe. To obtain $Fe^{3+}/\sum Fe$, FeO was analyzed by volumetric (titration) method. H_2O+, H_2O- were obtained by heating at 100°C and 1000°C (volumetric method), and CO_2 was analyzed by coulometric method (CRPG).

found for the samples from dredge 105. The change in fO_2 depends on the volatile content of the melt (H_2O, CO_2;) [*Byers et al.*, 1984]. The volatile content (i.e. H_2O=2-3% and CO_2=0.28-0.9%) of the dacites (samples 91-01 and 86-02) and andesite 92-02 is comparable to that of the other silicic lavas (andesites sample 105) and is higher than that of the MORBs. The samples (91-06, 86-02 and 92-03) with higher $Fe^{3+}/\Sigma Fe$ (0.13-0.16) ratios which also depart from the other trends of fractionation (QMF=0 and -1) have probably gained oxygen from ferromagnesian silicates rather than from primary dissolved volatiles in the melt.

The silicic lavas (andesite sample 92-02, dacite sample 91-01 and dacite sample 86-02) departing from the main fractionation trends lie on a mixing curve between the least evolved PAR MORBs and the other silicic lavas (dredge 105 and sample 92-01) depleted in TiO_2 (<2%) and FeO total (<10%) (Figure 3a and 3c). The calculated mixing curve shows a close fit when 75% of MORB is mixed with 25% dacitic melt (Figures 3a-3d). These silicic lavas were produced either from the remelting of a previously highly fractionated felsic lithosphere in the sense postulated by *McBirney* [1993], or during an *in* situ crystallization process in a large steady-state magmatic reservoir. During the solidification of the magma chamber walls (boundary layer or in situ crystallization of *Langmuir* [1989], evolved melts are produced in the solidification zones. If these melts are removed from the crystallization zone, they could mix with the main magma body present in the inner part of the reservoir and give rise to the silicic lavas with intermediate compositions. Another possibility is that they are formed by a simple mixing between a fractionated melt and a lesser evolved convecting liquid in a large magma chamber. The liquids giving rise to samples from dredge 92, except for sample 91-01 have reached a maximum enrichment in Ti and Fe earlier during the process of crystal fractionation than the other silicic melts (i.e. dredges 105 and 91). This is due to the fact that crystal fractionation took place in a more oxygenated environment and the production of these silicic lavas gave rise to a higher Mg # (35-40) than the others (Figures 3a and 3d). Indeed, when plotting a strongly incompatible element such as Ni it is observed that the andesite (sample 92-02) falls on the expected trend of crystal fractionation shown by other East pacific Rise (EPR) and PAR samples (Figure 3e).

Oblique Ridges

The Oblique Ridges are linear structures of about 100 km in length and 30-40 km wide with two sets of directions: 075° at 100-130 km located at dredge sites 71 to 74 (112-114°W) and 120° located at dredge sites 75 to 87 (111°30'-112°W) at less than 306 km from the PAR axis (Figure 1). These structures are characterized by the presence of volcanic cones which coalesced together forming single linear structures (Figure 1). The set of Oblique Ridges nearer to the PAR axis (oriented at 120°) are, in general shallower (1600-1700 m) than that of the average PAR axis depths (2200-2400 m) [*Devey et al.*, 1997]. The volcanic cones forming the other set of Oblique Ridges (oriented at 075°) are generally shallower (1300-1650 m) than those oriented at a 120° direction.

Rock types. The Oblique Ridges consist of N MORB (samples 74-01, 74-02, 74-03, 74-04 and 79-06), T-MORB (samples 75-01, 78-01, 82-02, 83-01, and 84-01) and enriched (E) MORB (samples 71-01, 71-02, 76-04, 87-01) (Table 3). The E MORBs have a K/Ti ratio of 0.20-0.30 and total alkali (Na_2O + K_2O) of 3.3-3.6% (Fig. 6a and 6b). Samples 74-01, 74-02, 74-03, 74-04 and 79-06 have low K_2O (< 0.04), and low K/Ti (< 0.06) and Ca/Al (<0.86) ratios and high MgO (> 9 %) content of their glass (Table 3). These samples consist of abundant olivine (>7 %) and spinel and are considered as picritic basalts Trace element analyses on bulk rocks show Zr and Y values of 72-87 ppm and 22-26 ppm respectively for T MORB, 140 ppm and 34-40 ppm for E-MORB (samples 87-01, and 73-04), and 32 ppm and 6-21 for N MORB (Table 5a and 5b and Figures 6a and 6b). The Oblique Ridge basalts show similar compositional variabilities of their incompatible element ratios K/Ti, Zr/Y-Zr, and $(Ce/Yb)_N$ to the PAR samples as well as to what is observed in other South East Pacific Rise segments (Figures 6a, 6b, and 7a-7d). The flat REE distribution is comparable to that of the PAR MORBs except for the picritic samples (samples 74-04, 74-06 and 79-06; see Figures 4a and 4b).

Magmatic processes. When modeling crystal fractionation, most Oblique Ridge volcanics fall close to the the liquid line of descent obtained from the fractionation of T MORB (i.e., sample 85-01). This is shown by the intermediate trend of TiO2 (2-3%) and Na_2O + K_2O variation with respect to their corresponding Mg #. The most depleted N MORB (i.e., sample 74-01) shows the lowest crystal fractionation trend among the volcanics collected from the various provinces. The calculated liquid line of descent enclosing the T and N MORBs indicates that plagioclase and olivine are the first to crystallize (5% crystallization). The trace element variation trend of moderately incompatible elements shows similar variability patterns. Most samples having a Zr/Y (3-4) and Zr of 80-87 ppm, $(Ce/Yb)_N$ of 2-2.3 and $(Ce)_N$ of 25-30 fall in a field of crystal fractionation defined by that of the T-MORB (i.e. 85-01) (Figure 6a and 6b). A few E MORB (samples 87-01, 76-04 and 73-04) departing from the other T MORB trend of variability are more enriched in total alkalies (Na_2O+K_2O=3-4%), and in their K/Ti (0.21-0.25), Zr/Y (sample 87-01=4.2) and $(Ce/Yb)_N$ (samples 73-04, and 87-01=2.3-3) ratios (Figures 5b, 6c and 6d). These samples may have resulted from magma mixing between an alkali basalt melt (i.e., 28-01, 58-01) and N, and/or T MORB type of melts (i.e., samples 74-01 and 85-01), or more likely from the partial melting of a heterogenous mantle source different from that giving rise to the other types of MORBs as shown by *Hémond and Devey* [1996]. An example of a heterogeneous mantle consisting of 85% lherzolite [*Frey et al.*, 1985] and 15% clinopyroxenite [*Irving*, 1980] mix was proposed (called 15/85 mantle source [*Hekinian et al.*, 1995a and 1995b; *Bideau and Hekinian*, 1995] as a potential source for some enriched MORBs from the SEPR. The melting curves calculated for the Ce_N versus $(Ce/Yb)_N$ and Zr versus Zr/Y falling close to the calculated mixing lines enclose the T and E MORBs (Figures 7a and 7b). The N MORBs are likely to have been derived from a more depleted source component than that used here. The alkali basalts are not produced from the same source as the MORBs but rather from a more enriched mantle source as will be discussed later.

Foundation Seamounts

The Foundation Seamounts (FS) are part of the FVC and consist essentially of isolated volcanoes located between longitudes 124°W and 115°W at about 410-1300 km from the PAR axis. The tallest edifices are found around 116°-117°W at dredge stations 67, 58 and 69 where shallow (180-700 m

Table 5a. Bulk Rock Trace Element Analyses of Intraplate and Off-Axis Volcanics From the South Pacific Near 37°S

	Old Pacific Seamounts			Foundation Seamount							
	T MORB			Trach A	Trach A	Alk B	Trach B	Alk B	Alk B	Trach A	Alk B
	11-03	11-04	18-01	25-01	25-08	28-01	38-01	41-04	46-03	58-02	70-01
SiO_2	48.30	46.50	49.50	58.00	58.40	48.50	47.00	42.60	45.60	55.00	46.90
TiO_2	1.82	1.72	2.33	0.92	0.96	2.45	2.20	3.20	2.75	1.82	2.35
Al_2O_3	15.15	14.20	15.30	16.50	17.10	15.70	21.10	16.20	17.70	17.00	14.70
Fe_2O_3	1.58	2.27	1.62	1.19	1.24	1.50	1.49	1.83	1.72	1.21	1.90
FeO	8.07	11.55	8.28	6.04	6.30	7.65	7.57	9.33	8.76	6.17	9.68
MnO	0.16	0.31	0.19	0.19	0.17	0.11	0.10	0.26	0.15	0.15	0.18
MgO	5.55	4.85	5.14	1.10	0.80	8.10	2.22	4.16	4.47	1.53	5.35
CaO	12.00	10.00	11.34	3.15	3.05	7.00	11.15	9.37	10.56	5.69	10.50
$N_{a2}O$	2.91	2.83	3.47	6.60	6.90	3.53	3.06	2.97	3.05	6.14	2.78
K_2O	0.44	0.87	0.42	2.85	2.94	1.62	0.64	0.83	0.46	2.26	0.70
P_2O_5	0.27	0.24	0.31	0.34	0.39	0.80	0.32	0.85	0.58	0.63	0.34
LOI	2.65	2.82	1.50	1.05	1.18	2.25	2.58	6.85	3.39	1.08	2.16
Total	99.80	99.42	100.32	98.60	100.13	100.06	99.43	99.49	100.16	99.36	98.61
Rb, ppm	11.0	20.0	5.5	28.0	28.5	27.0	14.0	38.5	4.6	26.5	11.5
Sr	183.0	184.0	304.0	258.0	275.0	542.0	578.0	570.0	498.0	370.0	280.0
Ba	26.0	43.0	61.0	590.0	575.0	305.0	97.0	127.0	118.0	432.0	96.0
V	295.0	286.0	300.0	14.0	62.0	147.0	202.0	212.0	232.0	53.0	305.0
Cr	150.0	120.0	34.0	2.0	0.0	232.0	15.0	48.0	160.0	2.0	70.0
Co	51.0	43.0	52.0	4.5	3.0	41 0	23.0	70!	34.0	8.0	44.0
Ni	52.0	74.0	40.0	3.0	17.0	192.0	16.0	80.0	70.0	5.0	55.0
Y	33.5	31.5	36.0	51.0	53.5	32.5	20.5	27.0	35.0	60.0	31.0
Zr	108.0	107.0	150.0	530.0	615.0	295.0	130.0	194.0	200.0	430.0	163.0
Nb	7.0	6.6	11.0	68.0	81.0	59.0	18.5	30.0	30.0	76.0	24.5
La	6.4	6.0	10.8	56.5	60.0	33.5	14.5	20.5	25.0	53.0	17.7
Ce	16.5	16.0	27.0	122.0	122.0	65.0	31.0	48.0	49.0	108.0	40.0
Eu	1.5	1.4	2.0	4.1	4.4	2.4	1.6	2.1	2.4	3.8	1.8
Dy	5.8	5.4	6.6	10.1	11.3	6.1	3.7	5.2	6.1	10.9	5.7
Er	3.4	3.2	3.7	5.2	5.8	3.1	1.9	2.7	3.4	5.9	3.1
Yb	3.2	3.0	3.4	4.5	4.8	2.6	1.6	2.0	2.7	5.2	2.8
Th	0.5	0.5	0.8	6.9	7.0	4.1	1.3	1.8	2.2	6.5	2.0
Mg #	57.66	45.40	55.16	26.50	20.09	67.71	36.73	46.89	50.27	32.95	52.27
Zr/Y	3.22	3.40	4.17	10.39	11.50	9.08	6.34	7.19	5.71	7.17	5.26
K/Ti	0.3	0.7	0.2	4.3	4.2	0.9	0.4	0.4	0.2	1.7	0.4
Ce_N	27.0	26.1	44.1	199.3	199.3	106.2	50.7	78.4	80.1	176.5	65.4
Yb_N	18.9	17.5	19.8	26.3	28.4	15.4	9.1	11.9	15.7	30.3	16.4
$(Ce/Yb)_N$	1.42	1.50	2.23	7.58	7.02	6.89	5.56	6.57	5.10	5.83	4.00
Distance km	1853	1853	1438	1212	1212	1332	1052	994	906	568	305

Trach A is trachyandesite, trach B is trachy basalt, and alk B is alkali basalt.

depth) topography was detected [*Devey et al.*, 1997]. Other shallow (300-1000 m depths) volcanoes are observed among the FS at dredge stations 25, 28, 38, 46, 58, 60, and 70.

Rock types. Several types of lava were recovered from the FS, the most prominent are the alkali basalts, trachybasalts and trachyandesites.

Alkali basalts: These are enriched in K_2O (0.5-1%) and K/Ti (> 0.3) ratios and mainly consist of porphyritic lava with up to 20% megacrysts and phenocrysts of plagioclase and olivine (Table 1). They include samples 70-01, 69-01, 60-05, 58-04, 46-02, 46-01, 38-02 and 28-01 (Table 3). Although sample 70-01 is considered to be an alkali basalt based on the

Table 5b. Bulk Rock Trace Element Analyses of Oblique Ridges Volcanics From the South Pacific Near 37°S and East Pacific Rise at 13°N

	Oblique Ridge MORBS									East Pacific Rise 13°N	
	E	N	N	T	T	T	N	T	T	Cy82-09-03	
	73-04	74-04	74-06	75-01	75-02	78-02	79-06	83-02	87-01	Mean	Standard Deviation
SiO_2	44.00	45.30	46.00	49.30	49.80	49.30	46.75	49.70	49.60	49.54	0.27
TiO_2	2.45	0.74	0.74	1.30	1.33	1.22	1.19	1.39	2.16	1.78	0.05
Al_2O_3	14.30	16.73	16.60	15.45	15.93	15.65	16.55	15.39	14.15	16.25	0.57
Fe_2O_3	2.12	2.02	1.98	1.47	1.37	1.52	1.57	1.61	1.96	nd	nd
FeO	10.80	10.32	10.10	7.50	6.99	7.73	8.02	8.20	9.98	8.63	0.30
MnO	0.32	0.22	0.21	0.22	0.15	0.17	0.16	0.18	0.21	0.13	0.08
MgO	5.08	10.30	10.80	6.93	7.30	7.24	11.05	7.40	6.08	7.70	0.06
CaO	10.40	10.25	10.48	12.80	13.40	12.80	10.75	12.00	10.64	11.21	0.21
Na_2O	3.23	2.47	2.38	2.51	2.49	2.32	2.81	2.70	3.01	3.10	0.10
K_2O	0.26	0.07	0.09	0.39	0.28	0.38	0.12	0.21	0.35	0.42	0.03
P_2O_5	0.55	0.13	0.10	0.14	0.14	0.13	0.13	0.15	0.26	0.25	0.02
LOI	4.67	0.53	-0.28	1.14	0.34	1.06	0.09	-0.16	-0.44	nd	nd
Total	99.12	100.23	100.32	99.98	100.30	100.37	100.08	99.68	99.07	99.01	
Rb, ppm	3.0	1.1	1.5	6.6	3.5	6.6	1.8	2.0	3.5	4.0	0.0
Sr	283.0	133.0	127.0	190.0	190.0	170.0	191.0	178.0	217.0	221.2	13.3
Ba	61.0	11.0	6.5	46.0	45.0	42.0	6.0	30.0	44.5	39.7	1.6
V	365.0	236.0	220.0	264.0	270.0	265.0	197.0	263.0	331.0	271.7	21.5
Cr	34.0	316.0	312.0	320.0	341.0	383.0	361.0	197.0	88.0	260.8	29.2
Co	90!	59.0	62.0	40.0	46.0	47.0	53.0	41.0	43.0	37.8	1.8
Ni	62.0	295.0	310.0	81.0	81.0	95.0	298.0	62.0	33.0	92.0	4.1
Y	43.0	22.5	21.5	23.0	23.5	22.0	25.0	24.5	33.0	34.2	2.5
Zr	135.0	32.0	32.0	80.0	83.0	72.0	85.0	87.0	140.0	148.8	7.2
Nb	17.7	1.4	1.4	8.4	8.5	10.4	2.2	7.0	12.0	nd	nd
La	16.5	1.8	1.9	7.0	7.2	8.0	3.3	6.5	11.3	8.0	3.3
Ce	36.0	3.7	5.0	16.0	16.5	17.5	10.5	15.5	26.0	22.6	1.4
Eu	2.0	0.7	0.7	1.1	1.2	1.1	1.1	1.2	1.7	1.2	2.0
Dy	7.1	3.5	3.4	4.0	4.0	3.8	4.0	4.2	5.8	nd	nd
Er	4.3	2.5	2.0	2.4	2.3	2.4	2.7	2.5	3.4	nd	nd
Yb	3.8	2.5	2.3	2.2	2.3	2.2	2.6	2.4	3.1	3.0	0.3
Th	1.3	0.1	0.1	1.0	0.7	1.0	0.2	0.6	1.0	0.6	0.1
Mg #	48.23	66.41	67.93	64.68	67.40	64.99	73.19	64.12	54.67		
Zr/Y	3.14	1.42	1.49	3.48	3.53	3.27	3.40	3.55	4.24		
K/Ti	0.1	0.1	0.2	0.4	0.3	0.4	0.1	0.2	0.2		
Ce_N	58.8	6.0	8.2	26.1	27.0	28.6	17.2	25.3	42.5	36.9	2.3
Yb_N	22.5	14.7	13.8	13.1	13.2	12.8	15.0	14.2	18.4	17.5	1.5
$(Ce/Yb)_N$	2.62	0.41	0.59	2.00	2.04	2.24	1.14	1.78	2.31		
Distance km	262	136	136	100	100	81	44	40	35		

E, N, and T indicate enriched, depleted, and transitional mid ocean ridge basalts (MORBs), respectively. Heading numbers refer to samples, and nd is no data. Standard deviations for the bulk rock aphyric sample Cy82-09-03 are from interlaboratory analyses.

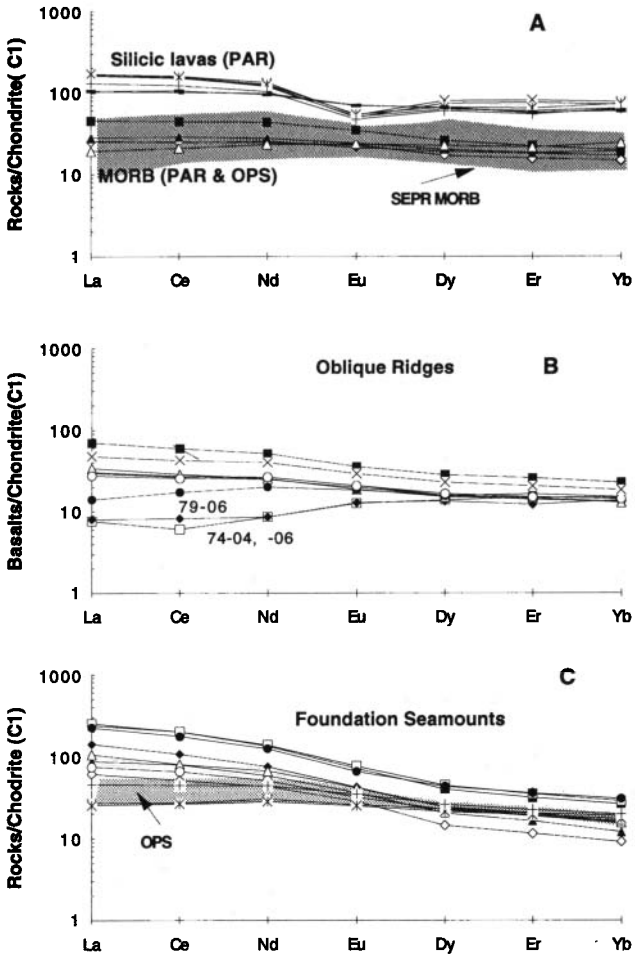

Figure 4. Rare earth element (REE) normalized to chondrite C1 [*Sun and McDonough,* 1989] distribution pattern of the bulk rock analyses of volcanics from the intraplate and spreading ridge (PAR) provinces of the South Pacific near 37°S. (a) Silicic and mid ocean ridge basalts (MORB) from the PAR and old Pacific seamounts (OPS) provinces. (b) Oblique Ridge MORBs. (c) Alkali basalt, trachybasalt and trachyandesite from the Foundation Seamount (FS) compared with the OPS lavas (shaded area).

high levels of incompatible trace elements (Zr/Y=5.26, $(Ce/Yb)_N$=4), the sample also has relatively low K_2O (0.55%) and K/Ti (0.29) values when compared with other E-MORBs (Table 3). The alkali basalts are also enriched in total alkalis ($Na_2O + K_2O$ =3-5%) and depleted in SiO_2 with respect those from the Oblique Ridges and PAR axis and are more comparable to hotspot volcanics from other south Pacific provinces (Figures 5a and 5b). They show an early crystallization of clinopyroxene-plagioclase-olivine and plagioclase-olivine and have the same olivine composition (Fo_{77-82}) as the other basalts, from which they differ only by the presence of a small amount of orthoclase in their plagioclase (Ab_{20-33}, An_{65-78}, Or_{1-2}). Among the alkali basalts, samples 38-02 and 60-05 are considered Fe-Ti enriched alkali basalts because of their high TiO_2 (3.3-4.5%) and FeO^T (>12%) (Table 3). They have a higher light REE (normalized to chondrite C1) pattern than the MORBs (Figure 4c).

Trachytic rocks: These are among the more evolved lavas (samples 25-01 and 58-02) erupted on the seamounts with high Na_2O (6-7%), K_2O (2-3%), and light REE concentration (La= 53-56, Ce=108-122, Nd=57-62) (Table 5). These samples have been discussed elsewhere [*Schuster,* 1996] and consist of sodic plagioclase laths showing fluidal textures.

Magmatic processes. The least-depleted glassy basalt sample 58-04 and the bulk rock sample 28-01 analyzed were chosen to calculate the crystal fractionation trends for the alkalic samples. Sample 28-01 is moderately phyric and contains olivine microphenocrysts (about 7%) as well as spinel, while sample 58-04 is a porphyritic and contains olivine and plagioclase phenocrysts. The glassy margin microprobe analyses for major and minor elements were used for calculating the trend of fractionation of the least evolved 58-04 sample. The alkalic trend defined by the glassy basalt 58-04 includes samples 46-02, 60-05, and 70-01 from the

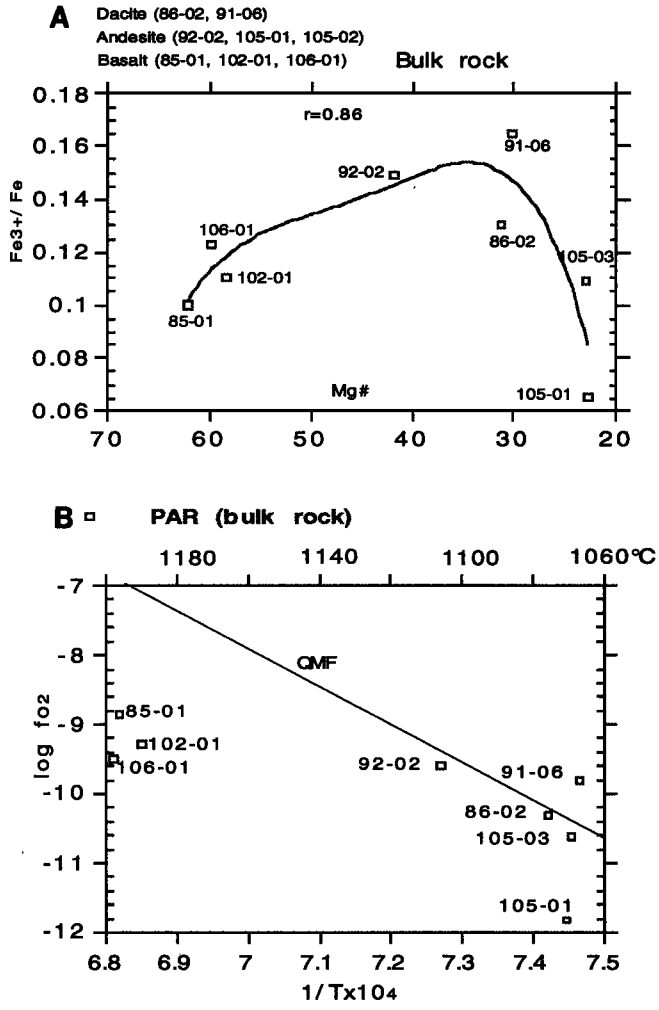

Figure 5. (a) $Fe^{3+}/\Sigma Fe$ atomic ratios versus Mg # of Pacific-Antarctic Ridge glass. The solid line is a best fit regression curve. (b) Log oxygen fugacity (fO_2) versus temperatures 1/T(t+273), where T=1348 x XMg+1069 x XAl+935.1 and X=mole fraction of oxide components.The quartz-magnetite-fayalite (QMF) buffer is obtained from experimental work and was used to control the oxidation of Fe (QMF=0) during crystallization modeling [*Wones and Gilbers,* 1969; *Sack et al.,* 1980; *Juster et al.,* 1989]. Most glassy samples lying below (reducing condition) the QMF line have lower $Fe^{3+}/\Sigma Fe$. Instead, the samples above or near the QMF line are more oxidized (higher $Fe^{3+}/\Sigma Fe$).

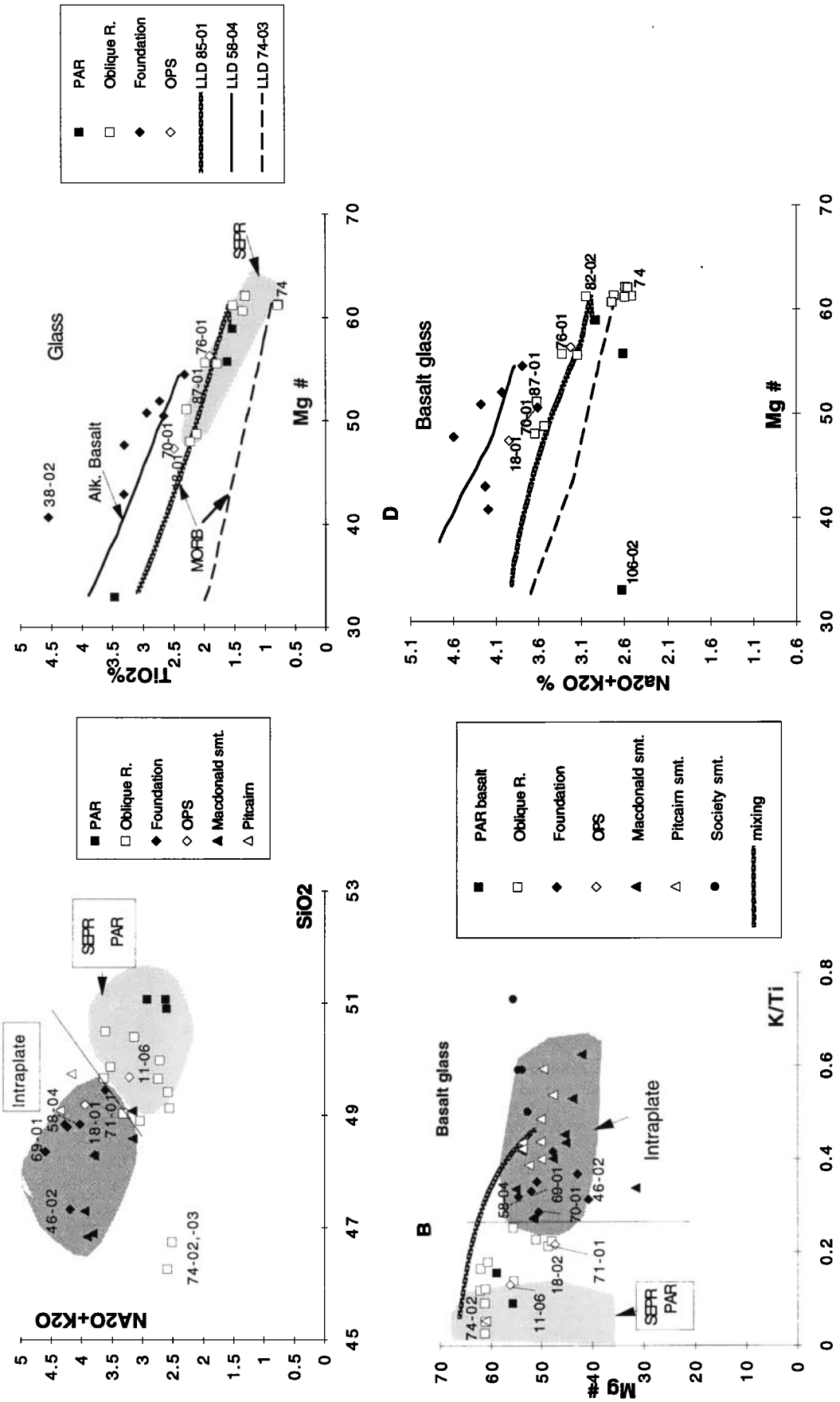

Figure 6. (a) $Na_2O + K_2O$ versus SiO_2 variations of glassy basalts from various South Pacific Intraplate and accreting ridge (SEPR, PAR) provinces. (b) Mg # versus K/Ti variation diagram. The mixing curve was calculated from some least evolved SEPR and intraplate (Pitcairn) basalts. The thin solid line represents an arbitrary separation of the accreting ridge volcanics from that of the intraplate provinces. The intraplate samples are all from submarine seamounts from various hotspots of the Society, Australs, Pitcairn [*Hekinian et al.*, 1991; *Ackermand et al.*, submitted manuscript, 1997] and Foundation Seamount (FS). (c) TiO_2 and (d) $Na_2O + K_2O$ versus Mg # variation diagrams of volcanics and crystal fractionation trends calculated from some least evolved liquids found on the Foundation Volcanic Chain seamounts (i.e., alkalic lava, sample 58-04), the PAR axis transitional (T) mid-ocean ridge basalt (MORB), sample 85-01 and an Oblique Ridge normal (N) MORB, samples 74-01, 74-02, 74-03). Symbols are the same as in Figure 5a.

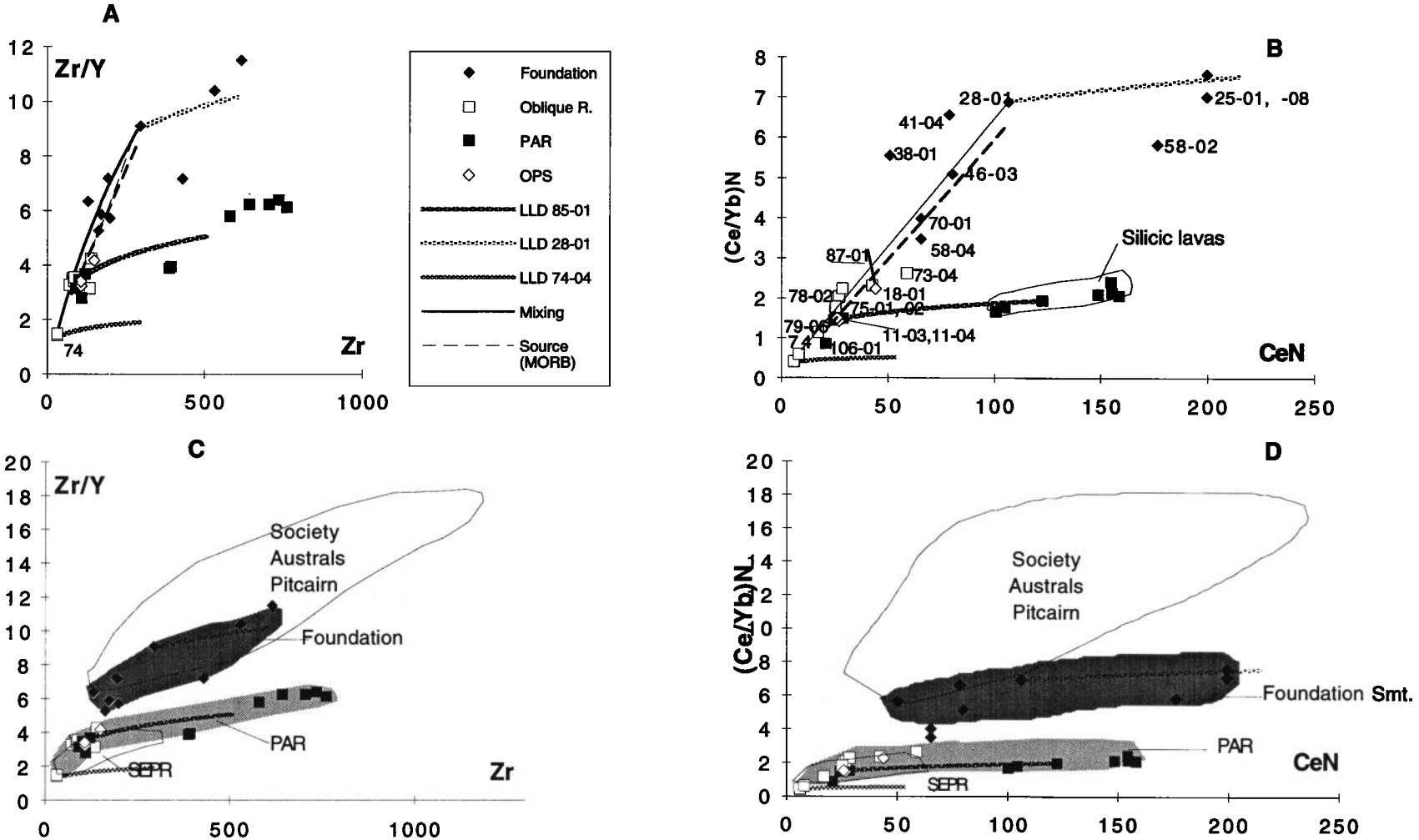

Figure 7. Trace element variations of the volcanics from the various South Pacific accreting ridge segments and intraplate provinces. (a) Zr/Y and (b) $(Ce/Yb)_N$ ratios of basalts and silicic lavas from the PAR axis, Oblique Ridges, Foundation Seamounts and Old Pacific Seamounts (OPS) (>23 m. y.). N indicates normalized to chondrite C1 [*Sun and McDonough*, 1989]. The calculated crystal fractionation, mixing and partial melting curves are shown. (c) Zr/Y and (d) $(Ce/Yb)_N$ ratios compared with other intraplate provinces [*Hekinian et al., 1991*; *Ackermand et al.*, submitted manuscript, 1997] and South East Pacific Rise (SEPR) segments at 7°S-29°S [*Bach et al.*, 1994], excluding the Easter and Juan Fernandez microplates. Samples 58-02, 25-01, and 25-08 are trachyandesites. A partial melting curve (stippled line) falling along the mixing curve was calculated for a nonmodal fractional melting model of a moderately enriched MORB mantle source (Zr=15 ppm, Y=6.3 ppm Ce=2.49 ppm, and Yb= 0.62 ppm) [*Hekinian et al.*, 1995b]. The source used consists of 15% spinel lherzolite and 85% clinopyroxenite (64% olivine, 17% orthopyroxene, 20% clinopyroxene, and 3% spinel).

seamounts. Other samples (69-01, 46-01, 38-02) which show higher values of total alkalies (4.3-4.6%) and TiO_2 (>3%) do not fall on this trend (Table 3, Figures. 6a and 6b). Another trend of crystal fractionation defined by a more enriched parental melt (i.e., sample 28-01) than sample 58-04 gives rise to a more enriched liquid line of descent. This is observed in the variation of the bulk rock trace element Zr/Y (7-10) and $(Ce/Yb)_N$ (6-7) ratios for some of the alkalic samples (samples 41-04, 25-01, and 25-08) (Figures 6a and 6b).The calculated alkalic liquid line of descent of the least evolved samples indicates that plagioclase is the first mineral to crystallize, followed by the cotectic crystallization of olivine and clinopyroxene (5-6% crystallization). The melting curves calculated from the mixed source model (15/85 mantle source) for the Ce_N versus $(Ce/Yb)_N$ and Zr versus Zr/Y encompass all the alkali basalts from the FS area (Figures 7a and 7b). When comparing the compositional variation of the FS to other volcanic provinces, the FS volcanics are included in the lower part of the incompatible element fields of other intraplate hotspots from the South Pacific (Figures 6c and 6d).

Old Pacific Seamounts

The Old Pacific Seamounts (OPS), are located between 32°40'S-131W and 33°30'S-126°W (at dredge stations 11 and 13 to 19), more than 1300 km from the PAR axis, on a crust older than 23 m. y. and probably formed when the Pacific fracture zones had a "Farallon plate" orientation (Figures 1b and 1c). They have similar structures to shallow (700-1700 m depths) edifices such as the FS, from which they differ by their composition.

Rock types. Most samples studied are from dredges 11 and 18 and consist essentially of aphyric lavas with few microphenocrysts of plagioclase and olivine (Table 1). Some samples contain megacrysts (xenocrysts or foreign inclusions) of plagioclase set in a basaltic matrix of plagioclase and olivine microlites [*Schuster*, 1996]. The few basalts with preserved glassy rims consist of T (sample 11-06), and E (sample 18-01) MORBs. They have a K_2O of 0.18-0.40%, K/Ti of 0.13-0.22, and a $Na_2O + K_2O$ of 3-4% (Table 3). The bulk rock analyses of the freshest samples (11-03, 11-04, and 18-01) also indicate that they are T and E MORBs with Zr of 100-150 ppm and Ce_N of 16-45. The T MORBs with Zr/Y (3.2-3.4) and $(Ce/Yb)_N$ (1.4-1.5) ratios fall in the fields of other PAR and Oblique Ridge volcanics (Figures 7a and 7b). The OPS show a flatter light REE pattern of variation than that of the FS (Figure 4c).

Magmatic processes. Crystal fractionation and magma mixing giving rise to the OPS samples are believed to be similar to that of the Oblique Ridges and PAR volcanics. The moderately evolved (Mg #=47) T MORB (sample 11-06) falls in the calculated trend of crystal fractionation defined by the T MORB (sample 85-01) from the PAR axis (Figure 6c and 6d). The E MORB (sample 18-01) has high TiO_2 (2.49%), and $Na_2O + K_2O$ (3.92%) contents and falls in an intermediate field between the T-MORB and alkali basalt liquid line of descent (Figures 6c, 6d, 7a and 7b). This is best evidenced by the relatively high $(Ce/Yb)_N$ (2.2) and Zr/Y (4.17) ratios of sample 18-01 when compared to the other types of MORBs (Table 5a and 5b and Figure 6c).

Regional Variations Between Pacific-Antarctic Ridge and Intraplate Volcanism

The first alkalic lavas found on the FS province were recovered at dredge site 28 (sample 28-01), which is believed to coincide with the beginning of the hotspot in the area about 23 m. y. (Table 1 and figure 1b). Lava morphology and structure vary between the PAR axis, the Oblique Ridges and the OPS basaltic flows on one side and the FS volcanics on the other. Dredge stations 11 and 18 located at about 1851 km and 1436 km respectively, away from the PAR axis were taken from the flank of relatively shallow (1500 and 840 m depths) edifices on the OPS (Figures 1b and 1c). These volcanics are coated with Fe-Mn crust and consist of both aphyric and highly phyric plagioclase basalt (HPPB) pillows which are moderately (<10 % vesicles) to rarely vesiculated (<1% vesicles) (Table 1). The samples from FS at 310-1300 km from the PAR axis (dredge stations 28 to 70) are highly phyric and highly vesiculated lavas in most cases (except for samples 69-01 and 28-01). The samples from these various dredge hauls are coated with Fe-Mn and palagonatized crust, suggesting that they are relatively old volcanics. The freshest samples of the FS are found in dredges 69 and 70 [*Devey et al.*, 1997] nearer to the Oblique Ridges. The PAR lava, and samples from the oblique ridges (<410 km from the axis) from stations 71 to 87 (including 97) (37°S-115°W and 37°S-111°W) also contain less vesicular and less phyric basalt flows than the basalts from the other seamounts in the OPS and FS provinces. Another major difference between the FS, the off-axis Oblique Ridges and the PAR axis is the increase in the size of the volcanic edifices from the axis up to about 1000 km away near 122°W [*Mammerickx*, 1992]. The seamounts of the OPS (700-1700 m depths) and FS (180-1000 m depths) are the shallowest edifices explored (Figure 1c). However, the PAR and the off-axis Oblique Ridges (up to 310 km from the ridge axis) show a deeper topography (1600-2300 m depths) (Table 1 and Figure 1c). In addition there is a general decrease of the topographic elevation between the volcanic cones of the Oblique Ridges (about 1600-1900 m) and that of the PAR axis (average depths of 2300 m) (Figure 1c).

The major compositional changes are observed between the FS seamount volcanics located between 410-310 km (stations 69 and 70) and 1332 km (stations 28 to 38) from the ridge axis and the other volcanics (Figures. 8a-8d). These FS volcanics consist essentially of alkali enriched lava with high $Na_2O + K_2O$ (3.5-5.0%), low Ca/Al (0.86-0.96) and high K/Ti (0.26-0.5 %) values of their bulk and glass compositions (Table 3 and Figures 6c, 6d and 8a-8c). The relative decrease in Ca/Al ratios in the alkali-enriched lavas at the FS with respect to the basalts from the other provinces is primarily due to the crystallization of plagioclase which has lowered the Ca content of the liquid. Indeed, these alkali basalts contain abundant (> 20%) early formed plagioclase.

When approaching the PAR axis, there is a gradual change in the glassy basalt compositions between 310 (station 70) and 20 km from the ridge axis (i.e., at stations 71, 75, 76, 78, 82, 84, and 87) (Figure 8a-8c). This compositional change is emphasized by the decrease of K/Ti (0.12-0.26) and total alkali ($Na_2O + K_2O$ = 2.5-3%) and the increase in Ca/Al (> 1) ratios (Table 3, Figures 7a-7c). The seamounts built on the two sets of oblique ridges oriented at 075° and 120° located between 20 and 306 km from the axis at dredge stations 71 to 74, 75 to 87 and, 97 have erupted N (dredge 74 and sample 79-06) T- (75 to 84) and E (71, 76 and 87) MORBs (Table 3). The basalts from the PAR axis, consist of both depleted (N MORBs) and transitional (T MORBs) with K/Ti ratios of 0.09-0.16, total alkali content of less than 3%, high Ca/Al (1-1.15) and low Zr/ Y (2-4) ratios (Table 2 and Figures 8a-8d).

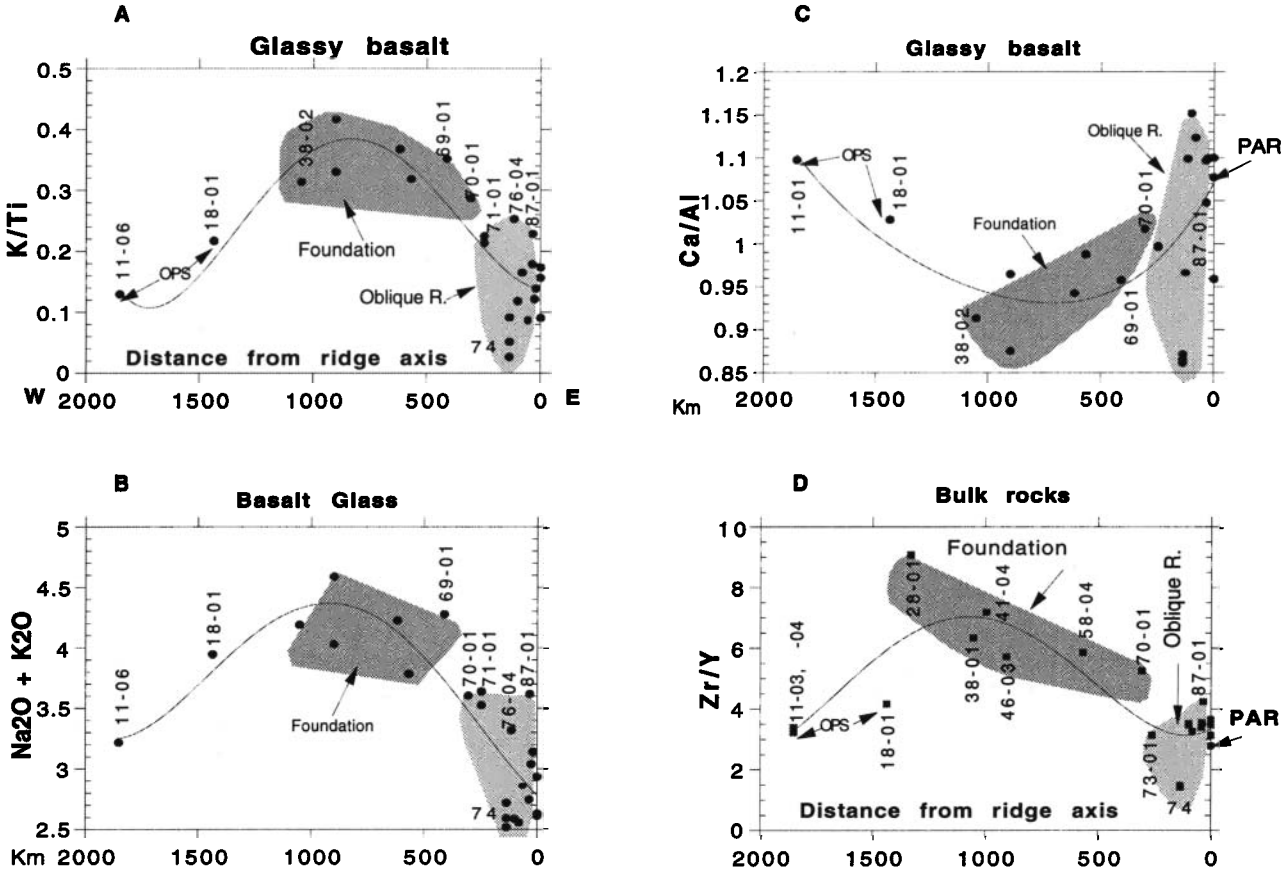

Figure 8. Regional compositional (a) K/Ti, (b) Na_2O+K_2O, (c) Ca/Al and (d) Zr/Y variation of the glassy basalts erupted along the Pacific-Antarctic Ridge, the Oblique Ridges (0-306 km), the Foundation Seamounts (FS), between 306 and 1300 km from the PAR axis and on the old pacific seamounts (OPS) constructed on the Farallon crust (>1300 km from the PAR axis). The best fit regression curve is constructed to guide the readers' eyes. (d) The Zr/Y ratio variation trends are from bulk rock analyses. Most samples lack glassy chilled margins and show some degree of alteration.

The gradual compositional changes observed could result the partial melting of mixed sources (heterogeneous mantle) giving rise to the alkali basalt (i.e. 28-01, 58-04, 69-01) the depleted MORB melts (i.e., samples 74-01, 85-01), the transitional (from dredge sites 75 to 84), and an enriched MORBs observed on the Oblique Ridges as well as their corresponding fractionated products (samples 71-01, 76-01, 87-1) (Figure 7a-7c). On the other hand, the most depleted and least evolved picritic lavas (MgO < 9%) from the Oblique Ridge (dredge 74 and sample 79-06) departing from the main variability trends by their lower Zr/Y (<2) and Ca/Al (< 0.9) are believed to have formed during a rapid magmatic ascent to the surface without undergoing crystal fractionation and/or mixing (Table 5a and 5b and Figure 8c and 8d).

Another compositional change occurs at dredge stations 11 and 18 (samples 11-06 and 18-02) collected from the OPS constructed on crust of more than 23 m. y. The samples consist of T and E MORBs with lower total alkali (< 4%) contents, lower K/Ti (< 0.22), higher Ca/Al (1.04-1.1), and lower Zr/Y (2-4) than the FS volcanics. The volcanics from the OPS are similar to those from the PAR and Oblique Ridges (Table 3 and Figure 7a-7c).

These regional compositional changes observed on the basis of the analyses of glassy margins are also emphasized by the bulk rock trace element contents of the various basalts. Thus the FS basalts have the highest incompatible element Zr/Y (5-9) and $(Ce/Yb)_N$ (4-7) ratios when compared to the other PAR, Oblique Ridges and OPS lavas (Zr/Y = 1-4.2; $(Ce/Yb)_N$ =0.4-2.5) (Figures 7c, 7d and 8d). The trace element variation such as Zr/Y (>5) and $(Ce/Yb)_N$ (>200) clearly shows that the most recent lava having the composition of an alkali basalt is located at 310 km from the PAR axis at dredge station 70 and those farther to the west (Table 5a and 5b and Figures 1b and 1c).

Discussion

The OPS volcanic structures were formed on an ancient lithosphere (>23 m. y.) located west of a large seamount (dredge station 28 near 34°S-125°W) which coincides with the trace of a failed rift [*Mammerickx*, 1992] and which is also the western boundary of the Silkirk microplate [*Tebbens and Cande* 1997] (Figure 1b). The samples analyzed from dredge hauls 11 and 18 of the OPS located between the Resolution fracture zone and 125°W (dredge 28) consist of T and E MORBs similar to those of the PAR and other Oblique Ridge volcanics, and it is likely that these volcanics are the result of similar magmatic processes of crystal fractionation and magma mixing at the source. However, because of their structural setting (presence of elevated edifices and a strike similar to the FS), it is not excluded that the OPS magmatism could also be related to the formation of the FS. It will be

necessary to obtain additional samples from the OPS before further speculating on their origin.

From our present data based mainly on the freshest bulk rocks and glassy margin analyses, the major compositional contrast between the PAR MORBs and the FS alkali basalts occurs between 411-306 km (116°W) and 1300 km (125°W) away from the accreting ridge axis (Figure 1b and Table 3). The compositional changes from alkali basalt to MORB correlate to a change in topography between the last volcanic event related to the formation of the last of the FS seamounts at dredge sites 69 and 70 and the PAR axis. This change in structure occurs at dredge sites 71 to 74 and 76 to 87, where the individual seamounts disappeared (dredge station 70) and where oblique trending ridges topped with volcanic cones extended to the PAR axis (Figure 1b). On the basis of a reconstruction of the Pacific-Antarctic plate using magnetic anomaly data [*Mayes et al.*, 1990] and assuming [*Searle et al.*, 1993] a half spreading rate of about 50 mm/yr for the Pacific plate, it is observed that at about 5 m. y. the seamounts of dredge stations 69 and 70 which are on a crust of age 5.8-7.7 m. y. (306-411 km from PAR axis), were in the position of the present-day dredge stations 75, 76, and 97 (110 km from the PAR axis) (Figure 1b, 8b, 9a and 9b). Because of the difference in the spreading rates (J. Morgan and P. Morgan, personal communication, 1996) between the Pacific (47 mm/yr) and the Antarctic (6 mm/yr) plates, the PAR axis is closer today to the FS hotspot (assuming the hotspot to be fixed).

The sets of Oblique Ridges (oriented 120° and 075°) corresponding to dredge sites 75 to 87 and 71 to 74, respectively, were possibly built during a period (1-5 m. y.) of intense activity related to the interaction of the hotspot plume and PAR magmatic upwelling systems (Figures 8a and 8b). The subsequent interaction between the FS hotspot and the PAR activities is marked by the presence of the Oblique Ridges, which could be associated with faults and fissures representing ridge axial discontinuities. Such structures may also be the traces of ancient leaky transform faults reoriented during the reajustment of the Pacific-Antarctic-Nazca plates in the last 5 m. y. The change in orientation of the Oblique Ridges west of the PAR axis is comparable to the directional changes observed west of the Easter microplate [*Hekinian et al.*, 1995a; *Searle et al.*, 1995; *Binard et al.*, 1997]. These types of elongated structures were inferred to represent leaky transform faults constructed within and/or at the edge of the microplate with continued volcanism during their westward drift. The construction of the Oblique Ridges corresponds roughly to the establishment of the Easter and Juan Fernandez microplates, 4-5 m. y. ago (chron 3) [*Searle et al.*, 1993]. However, we do not intend to correlate the Oblique Ridge

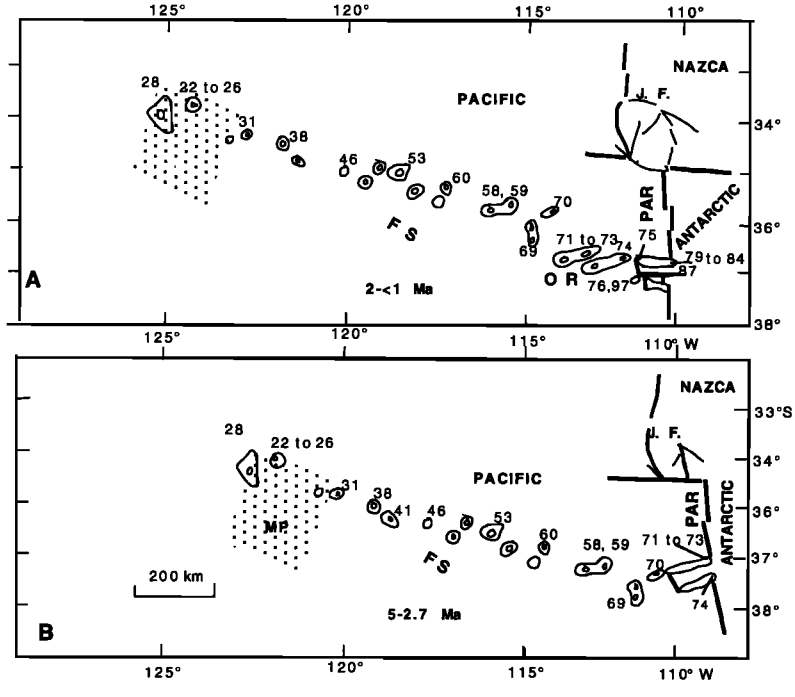

Figure 9. Reconstruction of the major volcanic structures using half spreading rates of 50 mm/yr [*Searle et al.*, 1993] from 5 m. y. to less then 1 m. y. This time span was chosen in order to include the formation of the two sets of Oblique Ridges and the last occurrence of alkali basalts on FS individualized volcanoes (stations 69 and 70). The scarcity of magnetic anomaly data makes it difficult to determine accurate reconstruction for this region. Also, it is assumed that the Pacific plate moves faster (47 mm/yr) than the Antarctic plate (6 mm/yr) (J. Morgan and P. Morgan, personal communication, 1996) and the PAR axis has come closer to the fixed hotspot of the FS. The Oblique Ridges (OR) oriented 075° (sample sites 71 to 73 and 74), and 120° (samples 79 to 84 and 87) were constructed at about (a) 2-<1 Ma and (b) 5-2.7 Ma. The off-axis Oblique Ridges represent ancient discontinuities (transform zones) filled by volcanic cones during lithospheric readjustment. This could either result from extentional or shearing motions of the Pacific-Antarctic-Nazca plates during the construction of small aborted microplates. The orientation of the Pacific Antarctic Ridge and the early formation of the Juan Fernandez microplate are inferred from the *Searle et al.* [1993] reconstruction. The location of the Skilkirk microplate (MP) is also indicated (Figure 1b).

structures to the above microplate; rather, we suggest that similar plate motions could have taken place during accretionary processes near 37°S. Also, it is not excluded that the set of Oblique Ridges could have been formed during the creation of small microplates which were aborted during spreading.

We did not find evidence of recent volcanic events at either the off-axial (<410 km from the axis) region along the Oblique Ridges nor in the intraplate regions along the FS. The hotspot was probably active within the Pacific plate (intraplate region), and it appears that contemporaneous magmatic upwelling also occurred underneath the PAR near 37°S until at least 5-7 m. y. This magma upwelling corresponds to the production of the alkalic lavas along the FS. Recent bathymetric and gravity anomaly studies [*Ito and Lin*, 1995] suggest that the influence of a mantle plume producing a hotspot will decrease with the increase of the ridge-hotspot distance owing to the cooling of the ridgeward migrating plume material.

An interaction between the mantle plume of the intraplate region and migrating ridge system was previously suggested by *Schilling* [1991], whose modeling showed that a migrating ridge is fed and dynamically affected by a plume flow at the base of the lithosphere. However, this theory has never been tested from field data along a continuous volcanic chain intersecting a spreading ridge axis.

The gradual change in composition from alkali basalts to less enriched MORBs suggests some extent of mixing between two types of mantle: (1) an enriched mantle source with high Zr/Y(>6) and Ce/Yb)N (>4), giving rise to the alkali basalts and (2) a more depleted source with lower in Zr/Y(<5) and Ce/Yb)N (<3), giving rise to MORBs (Tables 4 and 5b). Although E and T MORBS are found elsewhere along the SEPR, the higher $^{87}Sr/^{86}Sr$ isotopic ratio (0.7028) reported from a PAR axis lava [*Hémond and Devey*, 1996] makes this lava more comparable to that from the Easter microplate East Rift (0.7025-0.7026) [*Fontignie and Schilling*, 1991] than that from the SEPR, (0.7024-0.7027) [*Bach et al*, 1994; and *Mahoney et al*,. 1994;. *Fontignie and Schilling*, 1991] suggested that the East Rift volcanics are influenced by plume-generated melts.

Schilling's [1991] model of mantle plume source/migrating ridge sink (MPS/MRS) suggested that the plume source could feed and dynamically affect a plume flow at the base of the lithosphere. From our present observations it could be expected that the mantle plume producing the FS hotspot has also contributed to the formation of the Oblique Ridge-PAR volcanic structures. The decrease in incompatible elements (alkali components) toward the spreading center might indicate that all the MORBs found on the PAR and the Oblique Ridge, i.e., up to about 250 km (36°28-114°W, dredge 71) from the present-day PAR axis, were produced mainly during ridge-centered volcanism at 5 m. y.. This suggests that the mantle plume supplying the hotspot at that period and then located at about 110 km from the PAR axis at dredge site 69-70 was no longer as effective in melting enriched (with incompatible elements) component, and was gradually capturing and/or replacing the PAR spreading center magmatism (Figure 10a). This capture (at about 5m. y.) is interpreted as being related to the interaction of the FS plume with the PAR type of magmatism. Hence the mantle plume was gradually incorporating (mixing) more depleted mantle components from underneah the PAR axis around 5-7 m. y. (Figures 10b and 10c). Even if the eruption of alkalic lavas stopped (about 5-7 m. y.), this heterogeneous plume, located

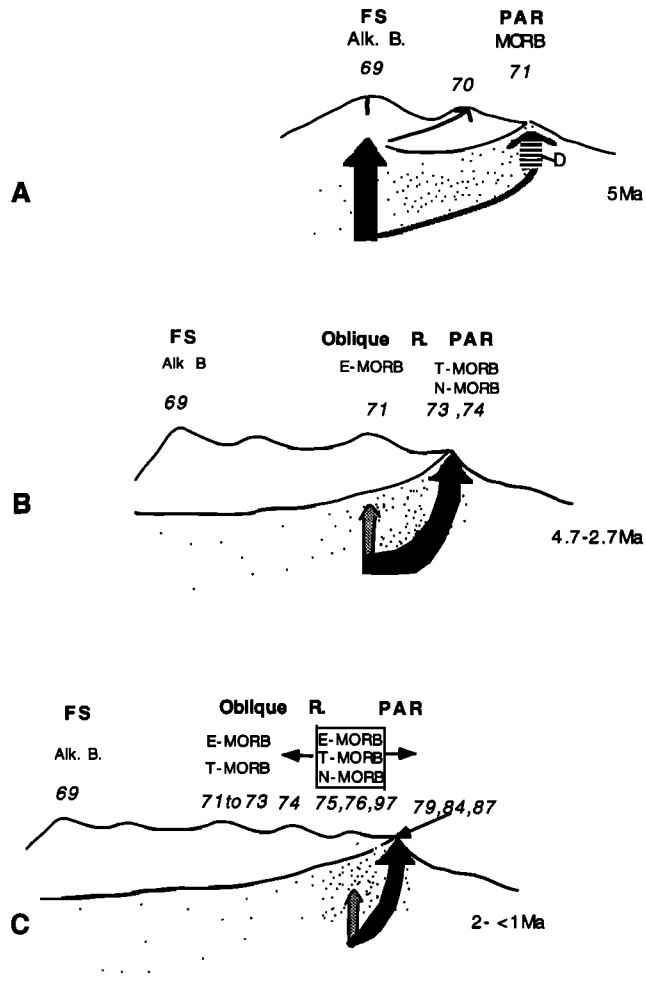

Figure 10. Sketched evolutionary model based on intraplate-ridge interaction between FS and PAR magmatism in the South Pacific near 37°S, assuming that the FS hotspot is fixed. Depleted melts are produced on the PAR axis (labeled D), while enriched magmas (alkali basalt) are formed underneath the FS (dredge stations 69 and 70) prior to 5.8 m. y. From 5.8 m. y. to less than 1 m. y. ago magma mixing (between depleted and enriched alkali basalt melts) have produced T and E MORBs. (a) The FS mantle plume underneath the hotspot (dredge sites 69 and 70) was captured by the PAR axis spreading centers, giving rise mainly to alkali basalts and E MORB at 5- 4.7 Ma. The formation of the first set of Oblique Ridges (oriented 070°) started at this period (about 5 m. y.) with the extrusion of MORBs (dredge site 71). The arrow underneath site 70 located near FS site 69 (<100 km) indicates a marginal volcanic event, giving rise to less enriched (K=0.55%, K/Ti=0.29) volcanics than those of most other FS hotspot volcanics. (b) The eruption of E, T and N MORBs on the Oblique Ridges occuring from the partial melting of a more ridge-centered heterogeneous mantle plume (old FS plume plus PAR mantle material) between 2.7 and 4.7 m. y. The trace of the older FS hotspot (arrow) is located underneath the Oblique Ridge at dredge site 71, and its influence (mixing) on the adjacent PAR magmatism could only be the result of magma channeling in the upper mantle. (c) The formation of the other set (oriented 110°N) of Oblique Ridges with a continued eruption of MORBs lasting until less than 1 m. y. At the present time the FS mantle plume (west of the PAR axis) might be still effective in maintainning high thermal conditions (dotted area) within the lithosphere at the level of the PAR segments between 36°S and 38°S.

west of the PAR axis and containing enriched and depleted components, has been effective in channeling within the upper mantle some enriched magma that has mixed with more depleted melts. Mixing is suggested by the gradual change in the incompatible elements towards the PAR axis and by the rather high strontium isotopic ratio found on a PAR sample [*Hémond and Devey*, 1996] with respect to other normal SEPR segments [*Bach et al.*, 1994]. Thus, the T and E MORBs from the Oblique Ridges and the PAR axis were produced from a mixing of at least two mantle sources during the interaction of the FS plume and the PAR axial magmatism. Also, because of the heterogeneous nature of the melting mantle, localized magmatic events of extremely depleted melts could explain the eruption of the N MORBs at dredge stations 74 and 97 on the Oblique Ridges. The presence of a hot mantle plume near and/or underneath the ridge axis could have maintained the thermal gradient (magmatic circulation in the upper mantle) and facilitate the presence of a steady state magma reservoir and the eruption of viscous lava. This situation is comparable to that of the Galapagos area where the eruption of silicic lavas was also suggested to be the result of hotspot influence [*McBirney*, 1993]. Also, the lack of surface evidence for recent FS hotspot and/or off-axis volcanic events does not exclude the possibility that intraplate magmatism could still occur and form dykes and sills intruding the lithosphere. The drastic changes in topography at a relatively short distance (30-150 km) between the Oblique Ridges (1500 m depths) and the PAR axis (2300-2600 m depths) also suggest that this heterogeneous mantle plume has been active until recently (Figures 1c and 10c). In fact, it is presumed that most of the mantle plume's activity is now ridge centered and flows along the PAR axis.

Conclusions

The interaction between a mantle plume of an intraplate region and a migrating ridge system is of prime importance understanding the behavior of deep-seated mantle plume upwelling underneath various structures forming the oceanic lithosphere.The present study is unique because it deals with a 2000 km long chain of seamounts intersecting a spreading ridge axis in the South Pacific near 37°S.

Four petrological provinces are recognized along the intraplate structures of the Foundation Volcanic Chain explored between the Resolution fracture zone near 32°56'-130°45'W and the Pacific-Antarctic Ridge near 37°30'-110°50'W (Figure 1): (1) the PAR axis segments, (2) the Oblique Ridges topped with volcanic cones, (3) the Foundation Seamounts between 34°15'S-122°14'W and 37°22'S-112°06'W, and (4) the Old Pacific Seamounts (>23 m. y.) located between 34°S-122°W and 32°56'-130°45W.

1. The PAR axis consists of several (5) ridge segments showing second- and third- order discontinuities, made up essentially of transitional MORBs, Fe-Ti basalt (sample 106-02), andesites (SiO_2 = 55-59 %), and dacites (SiO_2 = 60-65 %). Crystal fractionation of the least evolved T MORB melt has given rise to the various types of lavas. In order to produce the silicic lava, up to about 75% crystallization is necessary in a magma chamber. To explain the high degree of crystal fractionation, it is inferred that the Foundation Seamount hotspot environment generates a thermal flux toward the ridge which must have lasted up to the present day and which enhances the magmatic production responsible for erupting silicic lavas.

2. The Oblique Ridges located between 36°20'S-113°30'W and 37°30'-111°W (dredges 71 to 76 and 79 to 84, respectively) consist of linear structures about 100 km long and 30-40 km wide topped with volcanic cones made up of aphyric and moderately phyric MORBs. These structures are believed to represent ancient leaky transforms and/or fissures filled with volcanic cones constructed during an interaction between hot-spot plume material (sites 69 and 70) and PAR mantle products.

3. The Foundation Seamounts mainly consist of highly phyric and vesicular lavas of alkali basalt composition erupted on isolated seamounts (200-1000 m depths). From the present data the earliest volcanic event on the FS started near dredge station 28 at about 23 m. y.. It is believed that the last eruptive events of the FS hotspot took place in the vicinities of dredge sites 69 and 70, i.e., near 35°27'-36°33'S and 117°-115°W, located at about 410-306 km from the present-day PAR axis, about 5 m. y. ago. The change in structure from individualized seamounts to linear ridges taking place at less than 310 km from the PAR axis correlates with the change in compositional variations of the volcanics from alkalic lavas to MORBs. Foundation Seamount hotspot volcanism could have stopped with the last production of the alkali basalts (<5 m. y.) when it was replaced by magmatic upwelling underneath the PAR axis.

4. The Old Pacific Seamounts are the volcanic edifices built on an oceanic crust older than 23 m. y. located at more than 1400 km from the PAR axis and consisting of shallow (<1600 m depth) structures which are believed to have been built during the formation of an ancient ridge system at the time of the Farallon plate. The composition of the two glassy basalts (samples 11-06 and 18-01) recovered from these seamounts indicate the eruption of T and E MORBs. The bulk rock trace element and glassy margin analyses suggest similarities in the parental magma sources with those giving rise to the present-day PAR axis and Oblique Ridge volcanics. Whether these seamounts were constructed on off-axial regions or on an accreting ridge segment precursor of the present-day PAR is not yet well understood.

Crystal fractionation, magma mixing, and changes in the mantle melting conditions are the major magmatic processes involved in the petrogenesis of the volcanics erupted on the structures of the various provinces. Several fractionational crystallization trends are obtained when modeling on the basis of least evolved N MORB (sample 74-03), T MORB (i.e., 85-01) and alkali basalt (i.e., samples 58-01 and 28-01) as follows: (1) The most enriched alkalic trends enclude the FS basalt-trachyandesites. (2) The T MORB trend includes most Oblique Ridge basalts and PAR basalt-silicic lavas. (3) The most depleted N MORB trend comprises samples from dredge hauls 74 and 106 from the Oblique Ridge and the PAR sample respectively (Figures 6c and 6d). The decrease in alkalinity from the FS province (drege site 69 at 410 km from the ridge axis) to the Oblique Ridges (dredge sites 71-84 at 300-20 km from the ridge axis) and the PAR is believed to be the result of an interaction of the FS mantle plume with the PAR axis upwelling material. The FS mantle plume was captured by the PAR and/or replaced previous mantle upwelling underneath the PAR axis about 5 m. y. ago. Successive partial melting and melt extraction from a heterogenous plume source (mixed with alkali-rich and alkali-depleted components) gave rise to the Oblique Ridges and the PAR volcanics. The changes in topographic elevation between the Oblique Ridges (1500-1700 m) and the PAR axis (2300-2600 m depths) at about 30-100 km from the spreading center suggest that extensive volcanic activities probably due to the plume have continued to occur up to until now.

Acknowledgments. We are grateful to Capt. H. Andresen, and the officers and the crew of the R/V Sonne for their help and patience during leg 100. The cruise was funded by the German Ministry of Research and Technology (BMFT) and conducted by the Universität Kiel. This cruise was initiated within the framework of the French-German collaboration on Intraplate Volcanism. The microprobe analyses referred to in the text were performed with the technical help of M. Bohn on a Camebax SX50 at IFREMER. The bulk chemical analyses were done at the Centre de Recherche Pétrographique et Géochimique de Nancy (France) by induced coupled plasma mass spectrometric methods (ICP-MS) under the supervision of J. Morel and K. Govindaraju. We are indebted to IFREMER, CNRS, and Université de Bretagne Occidentale for their support. We are indebted to Jason Morgan for his encouragement and suggestions during the preparation of the manuscript. We are also very grateful to R. Batiza, A. C. Kerr, W.J. Hinze, and S. L. Goldstein for their helpful comments during the rewieving process.

References

Aumento, F., Diorites from the the Mid-Atlantic Ridge, Nature, 165, 112-113, 1969.

Bach, W., E. Hegner, J. Erzinger, and M. Satir, Chemical and isotopic variations along the superfast spreading East Pacific Rise from 6 to 30°S, Contrib. Mineral. Petrol.., 116, 365-380, 1994.

Batiza, R., Seamount and seamount chains of the Eastern Pacific, in The Eastern pacific Ocean and Hawaii, Geol. of North Am., vol. N, edited by E.L. Winterer, D.M. Hussong and R.W. Decker, pp. 145-159, Geol. Soc. of Am, Boulder, Colo., 1989.

Batiza, R., Y. Niu, J.L. Karsten, W. Boger, E. Potts, L. Norby, and R. Butler, Steady and non-steady state magma chambers below the East Pacific Rise, Geophys. Res. Lett., 23, 221-224., 1996.

Bideau, D., and R. Hekinian, A dynamic model for generating small-scale heterogeneities in ocean floor basalts, J. Geophys. Res., 100, 10,141-10,162, 1995.

Binard, N., P. Stoffers, R. Hékinian, and R.C. Searle, Intraplate en echelon volcanic ridges of the Easter microplate in the South Pacific, Tectonophysics, in press, 1997.

Byers, C. D., D. M. Christie, D. W. Muenow, and J. Sinton, Volatile contents and ferric-ferrous ratios of basalt, ferrobasalt, andesite and rhyodacitee glasses from the galapagos 95.5°W propagating rift, Geochim. Cosmochim. Acta, 48, 2239-2245, 1984.

Campbell, I.H. and J. A. Griffiths, Implications of mantle plumes for the evolution of flood basalts, Earth Planet. Sci. Lett. 99, 79-93, 1990.

Campbell, S., and W.F. Haxby, Eocene propagating rifts in the Southwest Pacific and their conjugate features on the Nazca plate, J. Geophys. Res. 96, 19,609-19,622, 1991.

Cande, S., and W. F. Haxby, Eocene propagating rifts in the Southwest Pacific and their cojugate features on the Nazca plate, J. Geophys. Res. 96, 1312, 19609-19622, 1991.

Carmichael, I.S.E. and M.S. Ghiorso, Oxidation-reduction relations in basic magma: A case for homogeneous equilibria, Earth Planet. Sci. Lett., 78, 200-210, 1986.

Christie, D.M., I.S.E. Carmichael, and C.H. Langmuir, Oxidation states of mid-ocean ridge basalt glasses, Earth. Planet. Sci. Lett., 79, 397-411, 1986.

Clague ,D.A., F.A. Frey, G. Thompson, and S Rindge, Minor and trace geochemistry of volcanic rocks dredged from the Galapagos Spreading Center: Role of crystal fractionation and mantle heterogeneity, J. Geophys. Res. ,86, 9469-9482, 1981.

Craig, C.H., and D.T. Sandwell, Global distribution of seamounts from Seasat profiles. J. Geophys. Res., 93, 408-420, 1988.

Devey, C. R. et al., Survey and sampling of the Foundation Seamount Chain, S.E. Pacific, Marine Geol., in press, 1997.

Fontignie, D., and J. G, Schilling, Sr/Sr and REE variations along the Easter microplate boundaries (South Pacific): Application of multivariate statistical analyses to ridge segmentation, Chemical, Geol. , 89, 209-241, 1991.

Frey, F.A., C.J. Suen, and H. W. Stockman, The Ronda high temperature peridotite: Geochemistry and petrogenesis, Geochim. Cosmochim. Acta, 49, 2469-2491, 1985.

Goldstein, S.J., M.R. Perfit, R. Batiza, D.J. Fornari, and M.T. Murell, Off-axis volcanism detected by uranium-series dating of basalts, Nature, 367, 157-159, 1994.

Govindaraju, K., Compilation of working values and sample description for 272 geostandards, Geostand. Newsl. 13, 1-113, 1989.

Haxby, W.F., Gravity field of the world's oceans,Report, U.S. Off. of Nav. Res, Arlington, Va, 1987.

Haxby, W.F., and J.K. Weissel, Evidence for small-scale convection from Seasat altimeter data, J. Geophys. Res., 91, 3507-3520, 1986.

Hémond C., and C. Devey, The Foundation Seamount chain: First isotopic evidence of a newly discovered hotspot track (abstract), presented at Goldsmitidt conference, Heidelberg 1, 255, 1996.

Hekinian, R., G. Thompson, and D. Bideau, Axial and off-axial heterogeneity of basaltic rocks from the East-Pacific Rise at 12°35'N-12°51'N and 11°26'N-11°30'N, J. Geophys. Res., 94, 17437-17463, 1989.

Hekinian R., D. Bideau, P. Stoffers, J.L. Cheminée, R. Muhe, and N. Binard, Submarine Intraplate Volcanism in the South Pacific: Geological Setting and Petrology, J. Geophys Res., 96, 2109-2138, 1991.

Hekinian, R., P. Stoffers, D. Ackermand, N. Binard, J. Francheteau, C. Devey and D. Garbe-Shonberg, Magmatic evolution of the Easter Microplate-Crough Seamount region (South East Pacific), Mar. Geophys. Res., 17, 375-397, 1995a.

Hekinian, R, D. Bideau, R. Hébert, and Y. Niu, Magmatism in the Garrett transform fault (East Pacific Rise near 13°27'S), J. Geophys. Res., 100, 10,163-10,185, 1995b.

Irving, A.J., Petrology and geochemistry of composite ultramafic xenoliths in alkalic basalts and implications for magmatic processes within the mantle, Am. J. Sc., 280, 389-426, 1980.

Ito, G., and J. Lin, Oceanic spreading center- hotspot interactions: Constraints from along isochron bathymetric and gravity anomalies, Geology, 23, 657-660, 1995.

Juster, T.C., T.L. Grove, and M.R. Perfit, Experimental constraints on the generation of FeTi basalts, andesites, and rhyodacites at the Galapagos Spreading Center, 85°W and 95°W, J. Geophys. Res., 94, B7, 9251-9274, 1989.

Kerr, A.C., A.D. Sounders, J. Tarney, V.H. Berry, and V.L. Hards, Depleted mantle-plume geochemical signatures: No paradox for plume theories. Geology, 23, 843-846, 1995.

Langmuir, C.H. Geochemical consequences of in situ crystallization. Nature, 340, 199-205, 1989.

Langmuir, C.H. , J.F. Bender, A.E. Bence, and R. Batiza, Petrological and tectonic segmentation of the East Pacific Rise, 5°30'-14°30'N, Nature, 332, 422-429, 1986.

Macdonald, K.C., R. Haymon, and A. Shor, A 220 km^2 recently erupted lava field on the East Pacific Rise near lat. 8°S, Geology, 17, 212-216, 1989,.

Mahoney, J. J., J. M. Sinton, M. D. Kurz, J.D. Macdougall, K. J. Spencer, and C. W. Langmuir, Isotopand trace elements characteristics of a super-fast spreading ridge: East Pacific Rise, 13-23°S, Earth. Plant. Sci. Lett., 121, 173-193, 1994.

Maia, M., and M. Diament, An analysis of the altimetric geoid in various wave bonds in the central Pacific Ocean: Constraints on the origin of intraplate features, Tectonophysics, 190, 133-153, 1991.

Mammerickx, J., The Foundation Seamounts: Tectonic of a newly discovered seamount chain in the South Pacific, Earth Planet. Sci. Lett. 113, 293-306, 1992.

Mayes, C.L., L.A. Lawver, and D.T. Sandwell, Tectonic history and new isochron chart of the south Pacific, J. Geophys. Res., 95, 8543-8567, 1990.

McBirney, A., Differentiated rocks of the Galapagos hotspot, in Magmatic Processes and Plate Tectonics, edited by H.M. Prichard, T. Alabaster, N.B.W. Harris, and C.R. Neary, Geol. Soc. Spec Publ., 76, 61-69, 1993.

Molnar, P., T. Atwater, J. Mammerickx, and S.M. Smith, Magnetic anomalies, bathymetry and the tectonic evolution of the south Pacific since the Late Cretaceous, Geophys. J. R. Astron. Soc., 40, 383-420, 1974.

Nielsen, R.L., A model for the simulation of combined major and trace element liquid lines of descent, Geochim. Cosmochim. Acta, 52, 27-38, 1988.

Nielsen, R.L., Theory and application of a model of open magmatic system processes, in Modern Methods of Igneous Petrology , Rev. Mineral., vol. 24, edited by J. Nicholls, J.K. Russell, pp. 65-106, Mineral. Soc of Amer., Washington, D.C., 1990.

Nielsen, R.L., and S.E. Delong, A numerical approach to boundary layer fractionation: Application to differentiation in natural magma systems, Contrib. Mineral. Petrol., 110, 355-369, 1992.

Sack, R.O., I.S.E. Carmichael, M. Rivers, and M.S. Ghiorso, Ferric-ferrous equilibria in natural silicate liquids at 1 Bar, Contrib. Mineral. Petrol., 75, 369-376, 1980.

Sandwell, D.T., A detailed view of the South Pacific geoid from satellite altimetry, J. Geophys. Res., 89, 1089-1104, 1984,.

Sandwell, D.T. and W.H.F. Smith, Marine Gravity Anomaly from Satellite Altimetry, Geol. Data Cent. Scripps Inst. of Oceanogr., LaJolla, Calif., 1995.

Scheirer, D. S., and K.C. Macdonald, Variation in cross-sectional area of the axial ridge along the East Pacific Rise: Evidence for the magmatic budget of a fast spreading center, J. Geophys. Res., 98, 7871-7885, 1993.

Schilling, J. G., Fluxes and excess temperatures of mantle plumes inferred from their interaction with migrating mid-ocean ridges, Nature, 352, 397-403, 1991.

Schuster, J., Mineralogy and geochemistry of the Foundation Seamounts (South East Pacific), M.A. thesis, 74 pp., Geosci. Mar. Univ. Bretagne Occidentale, Brest, France, 1996.

Searle, R.C., R.T. Bird, R.I. Rusby, and D.F. Naar, The development of two oceanic microplates: Easter and Juan Fernandez microplates, East Pacific Rise, J. Geol. Soc. London, 150, 965-976, 1993.

Searle, R.C., J. Francheteau and B. Corniglia, New observations on mid-plate volcanism and the tectonic history of the Pacific Plate, Earth Planet. Sci. Lett., 131, 395-421, 1995.

Shen, Y., Scheirer D.S., Forsyth D.W., and Macdonald K., Trade-off in production between adjacent seamount chains near the East Pacific Rise. Nature, 373, 140-143, 1995.

Sinton, J. M., S. M. Smaglik, J. J. Mahoney, and K. C. Macdonald, Magmatic processes at superfast spreading oceanic ridges: Glass variations along the East Pacific Rise, 13 S - 23 S, J. Geophys. Res., 96, 6133 - 6155, 1991.

Sun, S.-S., and W.F. McDonough, Chemical and isotopic systematics of oceanic basalts: Implications for mantle compositions and processes, in Magmatism in the Oean Basins, edited by A. D. Saunders and M. C. Norry, Geol. Soc. Spec. Publ., 42, 313 - 345, 1996,

Tebbens S.F., and S.C. Cande, Southeast Pacific tectonic evolutionfrom from early Oligocene to present, J. Geophys. Res., in press, 1996.

Thompson, G., W.B. Bryan, and S.E. Humphris, Axial volcanism on the East Pacific Rise, 10-12°N, in Magmatism in the Ocean Basins, edited by A.D. Saunders and M. Norry J.,Geol. Soc. Spec. Publ., 42, 181-200, 1989,.

Weaver, B.L., The origin of ocean island basalt en-member compositions: Trace element and isotopic constraints, Earth Planet. Sci. Lett., 104, 381-397, 1991.

Weaver, J. S., and C. H. Langmuir, Calculation of phase equilibrium in mineral-melt systems, Comput. Geosci., 16, 1-19, 1990.

White, R, and D. McKenzie, Magmatism at rift zones: The generation of volcanic continental margins and flood basalts, J. Geophys. Res., 94, 7685-7729, 1989.

White, W.M., Sources for oceanic basalts: Radiogenic isotopic evidence, Geology , 13, 115-118, 1985.

Wones, D.R., and M.E. Gilbert, The fayalite-magnetite-quartz assemblage between 600°C and 800°C, Am. J. Sci., 267 (A), 480-488, 1969.

Zindler, A., and S. Hart, Chemical geodynamics, Annu . Rev. Earth Planet. Sci., 14, 493-571, 1986.

R. Hekinian, Institut Français pour l'Exploitation de la Mer, Centre de Brest, Géosciences marines, 29280 Plouzané, France. (e-mail: hekinian@ifremer.fr)

P. Stoffers, C. Devey, J. O'Connor, N. Binard, University of Kiel Geologisch-Paläontologisches Institut, Kiel, Germany.

D. Ackerman, University of Kiel, Mineralogish-petrographisches Institut, Kiel, Germany.

C. Hémond and M. Maia, Département Sciences de la terre Université de Bretagne Occidentale, 6 Avenue le Gorgeu, Brest, France.

(Received July 8, 1996; revised December 2, 1996;
accepted December 9, 1996.)